Title
Synthetic Polymers for Mimicry and Modulation of Immunological Functions

Author
Santos, Giancarlo

Publication Date
2020

Peer reviewed|Thesis/dissertation

UNIVERSITY OF CALIFORNIA

Los Angeles

Synthetic Polymers for Mimicry and Modulation of Immunological Functions

A thesis submitted in partial satisfaction

of the requirements for the degree Master of Science

in Bioengineering

by

Giancarlo Santiago Santos

2020

ABSTRACT OF THE THESIS

Synthetic Polymers for Mimicry and Modulation of Immunological Functions

by

Giancarlo Santiago Santos

Master of Science in Bioengineering
University of California, Los Angeles, 2020
Professor Gerard Chee Lai Wong, Chair

Antimicrobial activity and smoking-induced inflammation are two seemingly disparate immunological phenomena in which the inherent heterogeneity of the system obfuscates the underlying fundamental mechanisms. Synthetic polymers represent a promising approach to simulating these systems. Here, a set of polyoxazoline-based synthetic antimicrobals exhibited a reversal in selectivity for Gram positive or Gram negative bacteria simply by tuning the ratio of hydrophilic to hydrophilic monomers. Small angle X-ray scattering (SAXS) reveals a link between bacterial selectivity and phase behavior. Additionally, a set of synthetic polymers recapitulating chemical motifs from tobacco alkaloids were shown to organize DNA. SAXS suggests that pH-dependent organization of DNA by these tobacco mimics is consistent with known mechanisms of immune hyperactivation and hyperinflammation. Overall, these results demonstrate the efficacy of synthetic polymers in emulating complex immunological phenomena and their potential for developing tunable, well-characterized systems that will allow for a better understanding of these phenomena in the future.

The thesis of Giancarlo Santiago Santos is approved.

Andrea M. Kasko

Timothy J. Deming

Gerard Chee Lai Wong, Committee Chair

University of California, Los Angeles

2020

Table of Contents

List of Figures

List of Tables

ACKNOWLEDGMENTS

The completion of this thesis would not have been possible without the help and support of many contributors. Firstly, I would like to express my deepest gratitude to my advisor, Dr. Gerard C.L. Wong. Before serving as the chair of my thesis committee, he was my assigned undergraduate faculty mentor. After persuading me to reconsider my plans for medical school (for which I am still grateful), I joined as an undergraduate researcher and eventually as a graduate researcher. He provided me the opportunity to develop my skills in a variety of research areas, including bacterial biofilms, mammalian cell culture, and small angle X-ray scattering. I have grown as a scientist through our many discussions and meetings, and I have always appreciated his interest in my well-being and life goals, in addition to my research progress. I would not have made it to this point, had it not been for his belief in me and my abilities. I also would like to express my deepest appreciation to the members of my thesis committee, Dr. Andrea Kasko and Dr. Timothy Deming, whose inputs and suggestions played an important role in the development of my thesis.

I would also like to thank all the members of the Wong Lab, including William Schmidt, Wei-chia Luo, Jaime de Anda, Calvin Lee, Ernest Lee, Michelle Lee, Yue Zhang, and Wujing Xian. I am deeply indebted to Ernest and Michelle for instructing me in the ways of small angle x-ray scattering, as well as to Calvin for his extraordinary patience in assisting me with MATLAB. Much thanks to Wei-chia, Jaime, and William for their companionship and our many conversations in the office and during our Stanford trips– graduate school would not have been nearly as memorable without them. Additionally, I very much appreciate the help from all the undergraduate researchers who helped me with cell stimulation experiments and X-ray data analysis, including Cole Malkoff, Mandy Hung, Eric Bilotta, Isabella Darke, and Yashes Srinivasan. Special thanks to Charles Lomba for his many puns and impromptu physics lessons.

I also had the great pleasure of working with members of the Kasko Lab. I am especially grateful for the help of Shadi Kordbacheh, who assisted me with performing specialized measurements on numerous occasions, as well as Sam Norris, who was always there to answer my questions and give practical advice. I cannot begin to express my thanks to Brooke Jackson and Shouzheng Yue for their commitment and dedication– they were always available to talk about anything and everything, and they never let me down.

Finally, I would like to extend my sincere thanks to my parents Will and Patti and my sister Kristen. My achievements would not have been possible without their unwavering encouragement and support throughout my educational career.

Sections of this thesis contain data gathered by collaborators or from published work:

Section 1: Tunable Antibacterial Selectivity of Poly-oxazolines– I would like to thank Dr. Runhui Liu and Min Zhou at East China University of Science and Technology (ECUST) for their contributions. Polyoxazoline polymer synthesis and bacterial killing assays were performed by Min Zhou. I acknowledge support from the NIH T32 Systems and Integrative Biology Training Grant at UCLA (T32GM008185).

Figure 1.1: Adapted with permission from N. W. Schmidt, A. Mishra, G. H. Lai, M. Davis, L. K. Sanders, D. Tran, A. Garcia, K. P. Tai, P. B. McCray, A. J. Ouellette, M. E. Selsted, and G. C. Wong, "Criterion for amino acid composition of defensins and antimicrobial peptides based on geometry of membrane destabilization," *Journal of the American Chemical Society*, vol. 133, pp. 6720–6727, may 2011. Copyright © 2011 American Chemical Society

Section 2: Smoking and Immunomodulatory Complex Formation– I would like to thank Dr. Andrea Kasko, Brooke Jackson, Shouzheng Yue, and Dr. Walter Liau at UCLA for their contributions. Characterization of tobacco total particulate matter, solvent extraction, and gas washing were performed by Brooke Jackson and Shouzheng Yue. Tobacco mimic polymers and their corresponding monomers were synthesized by Brooke Jackson. Brooke Jackson also provided the design for Figure 2.8. Glycopolymers and their corresponding monomers were synthesized by Dr. Walter Liau. Additionally, I acknowledge funding of this project by the Tobacco-Related Disease Research Program of California (TRDRP).

Figure 2.1: Adapted by permission from Springer Nature Customer Service Centre GmbH: Springer Nature, *Nature Materials*, "Liquid-crystalline ordering of antimicrobial peptide-DNA complexes controls TLR9 activation," N. W. Schmidt, F. Jin, R. Lande, T. Curk, W. Xian, C. Lee, L. Frasca, D. Frenkel, J. Dobnikar, M. Gilliet, G. C. L. Wong, Copyright © 2015

Section 1

Tunable Antibacterial Selectivity of Poly-oxazolines

1.1 Introduction

1.1.1 Antibiotics and Antimicrobial Peptides

Bacteria pose an enormous threat to public health, being the second-leading cause of death worldwide, superseded only by cardiovascular disease [1]. For the past 50 years, conventional antibiotics have filled the role of combating bacterial infections. Their targets include cell wall biosynthesis, protein synthesis, and DNA replication and repair [2]. Unfortunately, a subset of target bacteria will possess resistance genes, and those without them can acquire these genes through various gene transfer mechanisms, such as conjugation, transformation, and transduction [3]. Over the last 50 years, the overuse of conventional antibiotics has provided a selection pressure that facilitated the evolution of antibiotic-resistant bacteria. The infamous Methicillin-resistant *Staphylococcus aureus* (MRSA) was discovered in 1960 [4], the same year that Methicillin was released [5]. Antibiotic-resistant bacteria pose a significant threat to public health, causing approximately 2.9 million infections and 36,000 deaths in the United States in 2019 [5].

Antimicrobial peptides (AMPs) comprise a class of molecules with broad-spectrum activity against bacteria and other microbes. As naturally-occurring components of the innate immune system, AMPs typically serve as host defense peptides [6], though some may be pleiotropic [7]. The structures of AMPs range from the linear, α-helical LL37 to the rigid

β-sheet bactenicin and the cyclic, disulfide bond-stabilized RTD-1 [6]. Despite this diversity of structure, most AMPs possess a combination of hydrophilic, hydrophobic, and cationic amino acids and the ability to form amphipathic secondary structures, features that are critical for interactions with bacterial membranes [8]. In contrast to conventional antibiotics, the bacterial membrane serves as the major target of AMPs [8]. Due to the impracticality of reorganizing the bacterial membrane or altering membrane lipid compositions, genetic resistance towards AMPs is improbable [6], though other mechanisms for counteracting AMPs do exist [9]. These features of AMPs make them ideal model systems in the effort to develop more effective antibacterial agents.

1.1.2 Gram Positive and Gram Negative Bacterial Membranes

The structure of Gram Positive (Gr+) and Gram Negative (Gr−) bacterial outer membranes has significant implications for the design and mechanism of action of antibacterial compounds. Gr+ bacteria and Gr− bacteria both possess an inner membrane composed primarily of phospholipids, but their cell wall structures are markedly different.

For Gr+ bacteria, above the inner membrane is a thick layer of peptidoglycan (PG). PG consists of polymers of acetylated sugars, *N*-acetylglucosamine (NAG) and *N*-acetyl muramic acid (NAM). Each NAM molecule is attached to a short tetrapeptide, and crosslinks between tetrapeptides of adjacent polymers allow for the formation of a strong, rigid mesh-like network [10]. Though the thickness of the PG layer can reach 40-80 nm, it contains pores 4-5 nm in diameter [10] and is generally not considered to pose an obstacle to AMPs or objects of similar size. Another defining feature of Gr+ bacteria is teichoic acids (TAs), anionic polymers that extend outwards from the inner membrane or PG layer [11]. Wall teichoic acids (WTAs) are anchored to the PG layer and can extend beyond it, while lipoteichoic acids (LTAs) originate in the inner membrane and typically terminate in the PG layer [11]. Purportedly, TAs can either hinder or promote AMPs. For example, the strong electrostatic

interactions can facilitate the adsorption and subsequent immobilization of AMPs onto TAs, trapping them and preventing them from reaching the bacterial surface [12]. Alternatively, the TAs may present an "poly-anionic ladder" that only permits sufficiently (positively) charged molecules to reach the surface [12].

Gr− bacteria possess only a thin (3-10 nm) layer of PG above their inner membrane [13]. As with Gr+ bacteria, the PG layer is not believed to pose a significant obstacle to AMPs and their analogues. However, in contrast to Gr+ bacteria, Gr− bacteria contain an outer membrane, an additional lipid bilayer separated from the inner membrane by approximately 15 nm [13]. The anionic polymer in Gr− bacteria is represented by lipopolysaccharide (LPS). Each LPS molecule consists of three covalently bonded parts: lipid A, the core, and O antigen [14]. Lipid A consists of anionic sugars modified with long hydrocarbon chains, allowing for integration with the phospholipids in the outer membrane. The core is an oligosaccharide containing a mixture of anionic and uncharged modified sugars. The O-antigen is an uncharged glycan polymer forming the outermost portion of the LPS molecule, varying in length from one species to another. In contrast to the charges of TAs, which are distributed along the length of the molecule, the negative charges of LPS molecules are localized to the outer membrane surface, as they are contained within the Lipid A and inner core. Modifications to the charge and acyl chains of lipid A are known to alter membrane properties, thereby increasing evasion and decreasing the probability of an immune response [15]. In fact, the main permeability barrier to AMPs and similar molecules is due to LPS, namely the tight hydrocarbon packing of the lipid A moiety [16].

1.1.3 Mathematical Description of Membrane Disruption

Proposed mechanisms for AMP activity include the barrel-stave, toroidal pore, and carpet models [9, 17]. Each of these mechanisms specifies a method of membrane disruption via a particular spatial arrangement of membrane phospholipids.

Mathematically, membrane disruption can be described with the concept of Gaussian curvature from differential geometry [18]. On a differentiable 3D surface S, a point P can be chosen. There exists a unit normal vector $\hat{n}$ at point P, and by convention, it points "outwards". Next, a direction specified by the unit vector $\hat{v}$ can be specified, where $\hat{v}$ is perpendicular to $\hat{n}$. Point P and the points infinitesimally close to it (along direction $\hat{v}$) form a circular arc, which can be extrapolated to an entire [osculating] circle that has a radius R. Then, the curvature at point P in the direction $\hat{v}$ is simply given by $C = 1/R$. The sign of the curvature is positive if $\hat{n}$ points away from the center of the osculating circle, and negative otherwise. In general, the curvature at P takes on different values depending on the direction specified by $\hat{v}$. The minimum and maximum curvatures across all directions can be denoted C_1 and C_2, respectively. Then, the mean curvature H and Gaussian curvature K can be defined: $H = C_1 + C_2$ and $K = C_1 C_2$. Gaussian curvature, in particular, has implications for membrane deformation: negative Gaussian curvature (NGC) is necessary for membrane destabilizing processes [19] such as pore formation, blebbing, and budding(Figure 1.1B,C).

One method for detecting NGC in nanoscopic liquid-crystalline structures is small-angle X-ray scattering (SAXS). In SAXS, the objective is to solve the structure of a currently unknown sample. The sample is exposed to X-ray photons, which are scattered by atoms in the sample and collected by a detector. The resulting diffraction image is a cumulative count of scattered photons and their positions. If the sample is crystalline, the diffraction image will contain distinctive patterns of high intensity. Azimuthal integration of the scattered intensity transforms areas of high intensity into correlation peaks of varying width, height, and shape. It is through analyzing the characteristics of these peaks that the presence of various phases can be deduced, including the commonly-occuring lamellar, hexagonal, and cubic phases. In particular, the cubic phases that are often seen in biological liquid crystalline samples (Figure 1.1A) are rich in NGC, as they take the form of minimal surfaces [20]. The ability to form cubic phases (and thus generate NGC) when complexed with model bacterial

membranes is shared by many AMPs [19].

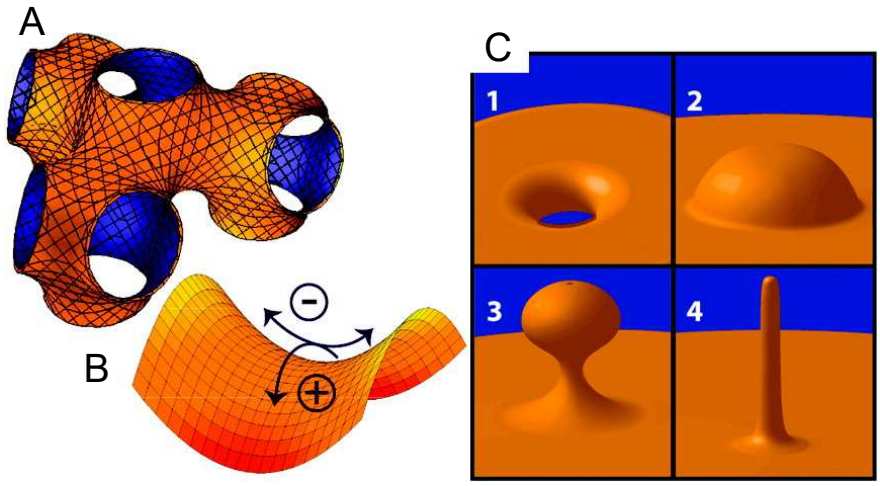

Figure 1.1: **Negative Gaussian Curvature**
Negative Gaussian curvature (NGC) is a prerequisite for various membrane deformation processes. (A) is an illustration of the *Pn3m* cubic phase, a minimal surface rich in NGC that commonly occurs in lipid-based liquid crystalline structures. The diagram in (B) represents the mathematical description of NGC, the product of two opposing curvatures (positive and negative). The panels in (C) depict membrane deformation processes that involve NGC, which is present at the interior of a pore (1) and at the base of blebs (2), buds (3), and rod-like projections (4).

1.1.4 Probing Anti-Bacterial Selectivity with Synthetic Poly-oxazolines

Synthetic polymer antimicrobials often attempt to recapitulate some of the defining features of AMPs: cationicity, and a mixture of hydrophobicity and hydrophilicity. These polymers vary widely in structure, from the identities of their hydrophilic and hydrophobic residues to their higher-order organization, which includes their classification as block, alternating, or random copolymers. Antimicrobial β-amino acid oligomers synthesized by Porter *et. al.* incorporate specific sequences that facilitate the formation secondary structures similar to

AMP amphiphilic α-helices [21]. A loss of secondary structure induced by scrambling the monomer sequence resulted in a loss of antibacterial activity [21]. Peptoids developed by Chongsiriwatana *et. al.* demonstrate antimicrobial activity whether the sequence facilitates amphipathic helix formation or is scrambled, suggesting that a well-defined secondary structure is not a necessary condition for antibacterial activity [22]. Other random copolymers, such as those synthesized by Kuroda *et. al.* and Mowery *et. al.* can also demonstrate antibacterial activity [23, 24].

Understandably, the goal of these synthetic antimicrobial systems is to design compounds with broad-spectrum antimicrobial activity that retain the functionality of AMPs but at a reduced cost. While some synthetic antimicrobials show preferential activity against either Gr+ or Gr− bacteria, a system with control over Gr+ and Gr− selectivity has not yet been investigated. Here, it is shown that a set of polyoxazoline-derived random copolymers constitute such a system. Each polymer is defined by the identity of its hydrophilic (3-aminopropyl) and hydrophobic (*n*-butyl, *i*-butyl, or *c*-butyl) group, as well as the overall ratio of hydrophilic to hydrophobic residues. The structure of these polymers is illustrated in Figure 1.2 and further detailed in Table 1.1. Polyoxazolines of varying hydrophilic/hydrophobic residue ratios are mixed with lipid vesicles mimicking bacterial membranes at different stoichiometries. Using bacterial killing assays, it is demonstrated that tuning the hydrophilic/hydrophobic residue ratio modulates the activity of the polymer against Gr+ and Gr− bacteria. Additionally, SAXS reveals that Gr+ selective polymers and Gr− selective polymers each have a distinct phase profile that yields mechanistic insights into their interactions with membranes. As a whole, this polymer system provides a platform for analyzing the role of hydrophobicity and charge in Gr+/Gr− bacterial selectivity.

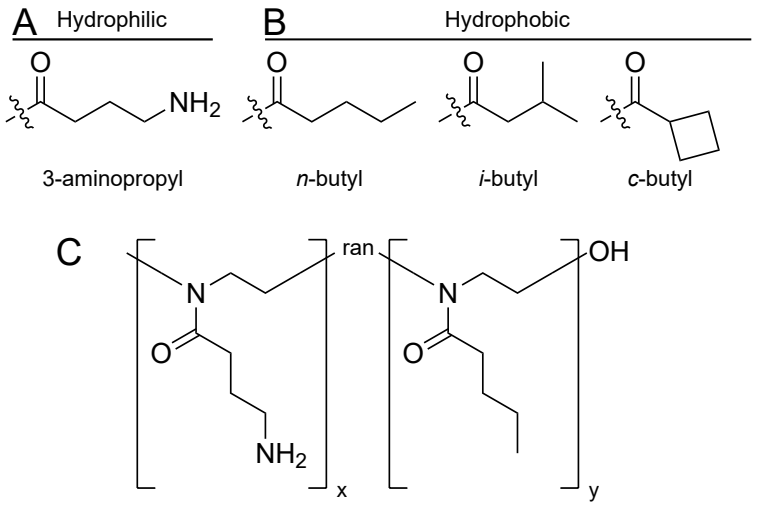

Figure 1.2: **Antimicrobial Polymer Chemical Structure**
(A) 3-aminopropyl serves as the sole hydrophilic and cationic side chain. For simplicity, the carbonyl is omitted in side chain nomenclature. (B) The hydrophobic side chain takes the form of one of these three butyl isomers: *n*-butyl, *i*-butyl, and *c*-butyl. In a given polymer structure, only one isomeric form is present. (C) This example polymer consists of x hydrophilic residues and y [*n*-butyl] hydrophobic residues, arranged randomly along an oxazoline-derived backbone. Any of the hydrophobic side chains in (B) can be used in place of the depicted *n*-butyl. A polymer structure is defined by the identity of its hydrophobic group and the average ratio of hydrophilic to hydrophobic residues x/y. A full list of polymer structures is given in Table 1.1.

Table 1.1: **Antimicrobial Polymer Structure Variants**

A summary of the various polymer structures. The polymers can broadly be classified into three groups according to the hydrophobic residue type. Within each of these groups, the ratio of hydrophilic to hydrophobic groups is adjusted while maintaining a constant degree of polymerization of $N = 20$.

Polymer Name	Hydrophobic Residue Type	Hydrophilic Residue Count, x	Hydrophobic Residue Count, y	Ratio x/y
ZM 2001-1	*n*-butyl	8	12	40/60
ZM 2018-5	*n*-butyl	12	8	60/40
ZM 2018-3	*n*-butyl	16	4	80/20
ZM 2054-2	*i*-butyl	8	12	40/60
ZM 2054-6	*i*-butyl	16	4	80/20
ZM 3116	*c*-butyl	8	12	40/60
ZM 2030-4	*c*-butyl	12	8	60/40
ZM 2030-6	*c*-butyl	16	4	80/20

1.2 Results and Discussion

1.2.1 Selective Antibacterial Activity by Tuning Monomer Ratio

The minimum inhibitory concentration (MIC) of each polyoxazoline was tested for various Gr+ bacteria (*Staphylococcus aureus* and *Staphylococcus epidermidis*) and Gr− bacteria (*Escherichia coli*, *Pseudomonas aeruginosa*, and *Acinetobacter baumannii*). A full list of MIC values is given in Table 1.2. Against a particular bacterium, any polymers with a MIC of 200 μg/mL or greater are considered ineffective.

Table 1.2: **Polyoxazoline MIC against Gr+ and Gr− Bacteria**

Gr+ bacteria tested were *S. aureus* (*S.a.*) and *S. epidermidis* (*S.e.*). Gr− bacteria tested were *E. coli* (*E.c.*), *P. aeruginosa* (*P.a.*), and *A. baumannii* (*A.b.*). x/y gives the hydrophilic/hydrophobic residue ratio, as in Table 1.1. Polymers are grouped according to the identity of their hydrophobic residues and ordered from lowest to highest hydrophilicity.

Data collected by Min Zhou, East China University of Science and Technology.

Polymer Name	Ratio x/y	MIC, μg/mL *S.a.*	*S.e.*	*E.c.*	*P.a.*	*A.b.*
ZM 2001-1	40/60	100	200	6.25	6.25	6.25
ZM 2018-5	60/40	50	50	50	25	25
ZM 2018-3	80/20	25	25	50	100	100
ZM 2054-2	40/60	200	200	25	25	25
ZM 2054-6	80/20	50	50	100	200	>200
ZM 3116	40/60	>200	>200	12.5	25	12.5
ZM 2030-4	60/40	100	100	50	200	50
ZM 2030-6	80/20	25	25	>200	200	200

A surprising pattern emerges when examining the effectiveness of each polymer against Gr+ and Gr− bacteria. The most hydrophobic polymers (x/y = 40/60) are effective against Gr− bacteria, but not Gr+ bacteria. For these hydrophobic polymers, MIC values against the Gr+ bacteria *S. aureus* and *S. epidermidis* were 200 μg/mL or greater (except for ZM 2001-1 against *S. aureus*, with MIC = 100 μg/mL). In contrast, MIC values against the Gr−

bacteria *E. coli*, *P. aeruginosa*, and *A. baumannii* were all 25 μg/mL or less. An opposite effect was observed with the most hydrophilic polymers ($x/y = 80/20$): they were effective against Gr+ bacteria, but not Gr− bacteria. For these hydrophilic polymers, MIC values against Gr+ bacteria were 50 μg/mL or lower, but 100 μg/mL or higher for Gr− bacteria (except for ZM 2018-3 against *E. coli*, with MIC = 50 μg/mL). Polymers with intermediate hydrophobicity ($x/y = 60/40$) have an effectiveness which does not suggest preferential activity towards either Gr+ or Gr− bacteria. MIC values for these intermediate polymers are largely in the range of 25-100 μg/mL.

While many AMPs (and their synthetic analogues) are effective against both Gr+ and Gr− bacteria, it is not uncommon for an AMP to have stronger activity against either class of bacteria. The reversal in bacterial selectivity that occurs with these polyoxazolines is unique because it occurs for both hydrophilic and hydrophobic polymers, and against both Gr+ and Gr− bacteria. In other words, varying the hydrophobicity and charge of the polymer confers effectiveness against one type of bacteria, but at the expense of effectiveness against the other. It may be argued that the ultimate goal of synthetic antimicrobial design is to engineer a compound that is effective against all bacteria. The selectivity reversal in these polyoxazolines, however, provides a platform that allows for the examination of hydrophobicity and charge in isolation.

1.2.2 Gram Positive Selective Polymers Generate NGC

To further explore the membrane deformation mechanisms that contribute to the bacterial selectivity, SAXS was performed on samples of polyoxazolines combined with small unilamellar vesicles (SUVs) mimicking bacterial membranes. SAXS data suggests that the polymers alone do not form ordered structures. When mixed with SUVs however, polymers form a mixture of lamellar and cubic phases. A full phase diagram is given in Table 1.3.

Table 1.3: **Phase Diagram of Polyoxazoline/Lipid Vesicle Mixtures**

Phase information is given for mixtures of polyoxazoline antimicrobials with vesicles of varying lipid composition. Lipid compositions and polymer to lipid (P/L) ratios are molar ratios. "L" indicates the lamellar phase and "Q(P)" and "Q(I)" indicate the Pn3m and Im3m cubic phases, respectively. Each group of polymers is arranged in order of increasing hydrophilicity. A complete description of each polymer is given in 1.1.

Polymer	P/L	DOPG/DOPE 20/80	DOPG/DOPE/DOPC 20/60/20	DOPS/DOPE 20/80
ZM 2001-1	1/40	L	L	L
	1/80	L	L	L
	1/160	L	L	L
ZM 2018-5	1/40	L	L	L
	1/80		L	L Q(P)
	1/160	L	L	L
ZM 2018-3	1/40	L	L	L
	1/80	L Q(P)	L	L Q(P)
	1/160	L	L	L
ZM 2054-2	1/40	L	L	L
	1/80	L	L	L
	1/160	L	L	L
ZM 2054-6	1/40	L	L	L
	1/80	L Q(P)	L	L Q(P)
	1/160	L Q(I)	L	L Q(I)
ZM 3116	1/40	L	L	L Q(I)
	1/80	L	L	L Q(I)
	1/160	L	L	L
ZM 2030-4	1/40	L	L	L Q(I)
	1/80	L Q(P)	L	L Q(P)
	1/160	L	L	L
ZM 2030-6	1/40	L Q(I)	L	L Q(I)
	1/80	L Q(P)	L	L Q(P) Q(I)
	1/160	L	L	L

The presence of cubic phases is correlated with total polymer hydrophilicity: cubic phases are more prevalent in polymer compositions that incorporate more hydrophilic residues. When samples are measured prior to incubation at 37°C, the difference is striking: no cubic phases occur in the most hydrophobic polymers ($x/y = 40/60$). Incubation allows cubic phases to form in some of the most hydrophobic variants, through the preference for cubic phases in hydrophilic variants remains apparent (note that all references to phase information hereafter will refer to post-incubation results). Even for hydrophilic variants, however, the presence of cubic phases is not universal. Rather, it depends on the stoichiometry between polymer and lipid: using more or less polymer can weaken the signal from cubic phases or cause cubic phases to disappear entirely.

For polymers containing *n*-butyl residues, cubic phases are not present for the most hydrophobic variant (ZM 2001-1, $x/y = 40/60$). One composition yields a cubic phase for the intermediate variant (ZM 2018-3, $x/y = 60/40$) and two compositions for the most hydrophilic variant (ZM 2018-3, $x/y = 80/20$). A similar trend emerges for polymers with *i*-butyl residues. No cubic phases are present in the most hydrophobic variant (ZM 2054-2, $x/y = 40/60$), while the most hydrophilic variant features four compositions with cubic phases (ZM 2054-6, $x/y = 80/20$). Polymers containing *c*-butyl residues have the greatest ability to generate cubic phases, which are present for all levels of hydrophobicity ($x/y = 40/60, 60/40, 80/20$).

The ability of hydrophilic variants to generate NGC is a trait shared with many AMPs [19]. In AMPs, the capability to generate NGC requires a balance of charge and hydrophobicity: lysine, arginine, and the hydrophobic amino acids must be present at the proper amounts for cubic phases to form [19]. Although the polyoxazolines may be seen as synthetic analogues of AMPs, the differences in polymer backbone structure, as well as differences between amino acids and oxazoline-derived monomers, make a direct translation of the hydrophilic/hydrophobic residue ratio difficult. Nevertheless, the general principle may still hold.

Hydrophilic variants possess the correct balance of hydrophobicity and charge to generate NGC, while intermediate and hydrophobic variants have a sub-optimal residue composition, which limits their ability to generate NGC. Additionally, the phase behavior of polymers with *c*-butyl residues appears distinct from those with *n*-butyl residues and *i*-butyl residues. In contrast to the *n*-butyl and *i*-butyl groups, the *c*-butyl group is more condensed by virtue of its ring, which results in an overall decrease in molar volume [25]. If hydrophobicity is viewed as a factor that stifles NGC generation, the decreased hydrophobic volume of *c*-butyl-containing polymers can explain the increased prevalence of cubic phases.

1.2.3 Gram Negative Selective Polymers do not Generate NGC, but can Abrogate NGC

SAXS reveals that polymer-lipid complexes form lamellar phases in virtually all combinations, regardless of stoichiometry or lipid composition (see Table 1.3). The lamellar distance is a lattice parameter obtained from analyzing SAXS data and represents the distance between the centers of two successive lipid bilayers. Typical phospholipid bilayers are 4 nm thick, but lamellar distances typically exceed 4 nm, as the space between two lipid bilayers is occupied by a water channel (whose thickness will be denoted the intermembrane distance). While 4 nm approximates the thickness of the model membranes used in this study, bacterial membranes are notably thicker, reaching 5-7 nm [26] or more due to the presence of membrane proteins and non-phospholipid components that promote membrane thickening.

Table 1.4: **Intermembrane Spacings**

Intermembrane distances are given as averages over polar to lipid molar ratios of 1/40, 1/80, and 1/160. The intermembrane distance is defined as the lamellar repeat distance, decreased by the thickness of a phospholipid bilayer (4.0 nm). Values are specified as mean ± S.D. in nm

Polymer Name	Ratio x/y	DOPG/DOPE 20/80	DOPG/DOPE/DOPC 20/60/20	DOPS/DOPE 20/80
ZM 2001-1	40/60	1.6 ± 0.6	1.7 ± 0.5	1.5 ± 0.3
ZM 2018-5	60/40		1.9 ± 0.1	1.7 ± 0.3
ZM 2018-3	80/20	1.8 ± 0.1	1.9 ± 0.1	1.9 ± 0.1
ZM 2054-2	40/60	1.7 ± 0.8	1.9 ± 0.7	1.6 ± 0.6
ZM 2054-6	80/20	1.8 ± 0.0	1.9 ± 0.1	2.0 ± 0.1
ZM 3116	40/60	2.3 ± 1.3	2.3 ± 0.5	1.9 ± 0.6
ZM 2030-4	60/40	1.9 ± 0.2	2.1 ± 0.0	2.1 ± 0.2
ZM 2030-6	80/20	1.9 ± 0.1	2.0 ± 0.0	2.1 ± 0.1

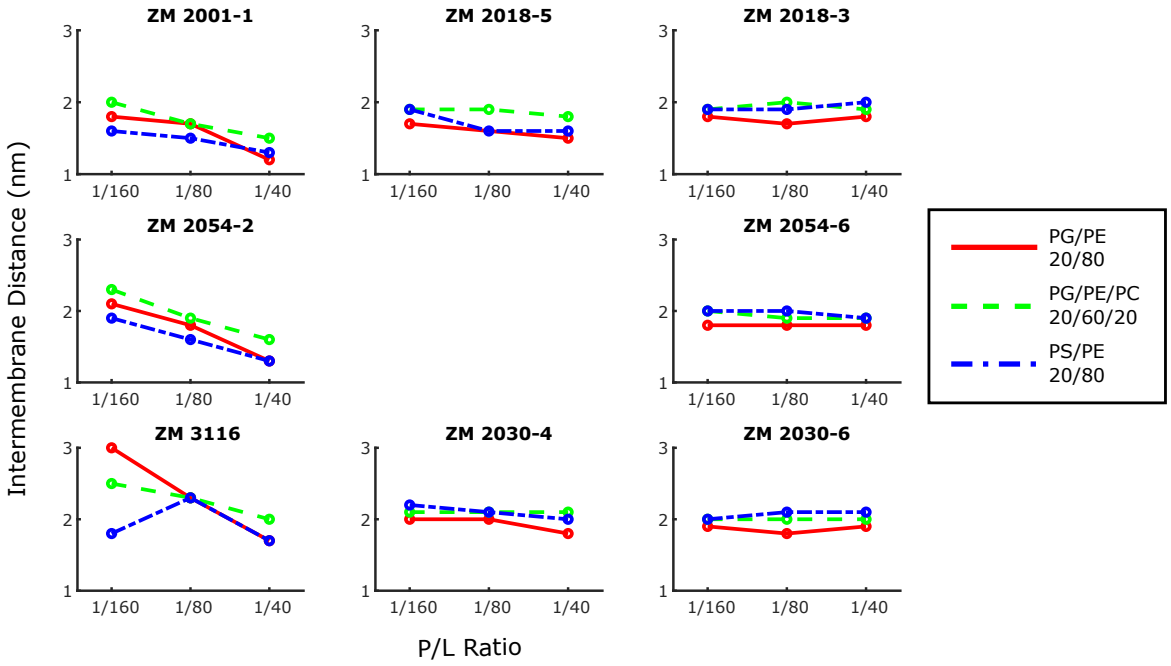

Figure 1.3: **Variations in Intermembrane Spacing**
The intermembrane distance varies with polymer type, lipid composition, and the polymer to lipid (P/L) molar ratio. Each row of plots represents a group of polyoxazolines with a shared butyl isomer. Within each row, polymers are listed from left to right in order of increasing hydrophilicty / decreasing hydrophilicity.

A full list of intermembrane distances is given in Table 1.4 and Figure 1.3. The most hydrophilic variants (x/y = 80/20: ZM 2018-3, ZM 2054-6, ZM 2030-6) exhibit only small fluctuations in intermembrane distance across different polymer/lipid stoichiometries. For this subset of polymers, the standard deviation does not exceed 0.3 nm. In fact, variations in intermembrane distances are not detectable for some mixtures (e.g. ZM 2054-6 with PG/PE 20/80, ZM 2030-6 with PG/PE/PC 20/60/20). In contrast, the most hydrophobic variants (x/y = 40/60: ZM 2001-1, ZM 2054-2, ZM 3116) exhibit relatively large fluctuations in intermembrane distance. The standard deviation of intermembrane distances over different stoichiometries varies from 0.3 nm (ZM 2001-1 with PS/PE 20/80) to 1.3 nm (ZM 3116 with PG/PE 20/80). The largest variations are observed in hydrophobic polymers containing *c*-butyl residues. Intermediate variants (x/y = 60/40: ZM 2018-5, ZM 2030-4) resemble their hydrophilic counterparts in terms of both mean intermembrane distances and the variation over polymer/lipid stoichiometries.

Lipid vesicles can also be mixed with multiple polymers, resulting in surprising behavior. Previously, it was noted that Gr+ selective polymers generate NGC over a wide range of stoichiometries and lipid compositions. This is the case for hydrophilic variants ZM 2018-3 and ZM 2030-6 when complexed with DOPG/DOPE 20/80 vesicles, which generate prominent cubic phases. Addition of the hydrophobic variants with matching hydrophobic residues (ZM 2001-1 and ZM 3116, respectively) into the system while holding the amount of hydrophilic variants constant has a marked effect on phase behavior. In particular, NGC is abrogated upon adding sufficient hydrophobic polymer. For ZM 2018-3, the transition is sudden: addition of ZM 2001-1 at P/L = 1/80 prevents the formation of a cubic phase. For ZM 2030-6, the cubic phase is at first weakened by the addition of ZM 3116 at P/L = 1/80 before vanishing when the amount of ZM 3116 is increased to P/L = 1/40.

Since NGC is a prerequisite for numerous membrane deformation processes, the presence of cubic phases has implications for the mechanisms by which polyoxazolines disrupt mem-

branes. However, the inability to generate cubic phases does not necessarily indicate the inability to kill bacteria. Hydrophobic variants ($x/y = 40/60$) can kill Gr− bacteria, despite their inability to generate NGC in model membranes (Tables 1.2,1.3). In contrast to the hydrophilic variants and many AMPs, hydrophobic variants disrupt membranes through a NGC-independent mechanism, perhaps one that cannot be detected using SAXS. Elucidating this mechanism would allow for the design of better synthetic antimicrobials that are able to overcome the unique challenges posed by both Gr+ and Gr− outer membranes.

In addition, these results suggest that the hydrophobic variants, when used in concert with hydrophilic variants, can have antagonistic effects. Antagonistic effects have been observed in conventional antibiotics since the discovery of penicillin, and antagonism is common in antibiotics with different mechanisms of action [27, 28]. Antagonism remains an important consideration as cocktail treatments for a variety of disorders become increasingly common [29–31]. The polyoxazoline variants, despite differing only in the ratio of hydrophilic to hydrophobic residues, also appear to operate via distinct mechanisms. Though the confirmation of antagonism between hydrophilic and hydrophobic variants would require additional bacterial killing assays, it is possible that a mixture of the two variants, rather than gaining the ability to kill both Gr+ and Gr− bacteria, would instead lose its activity against both classes of bacteria.

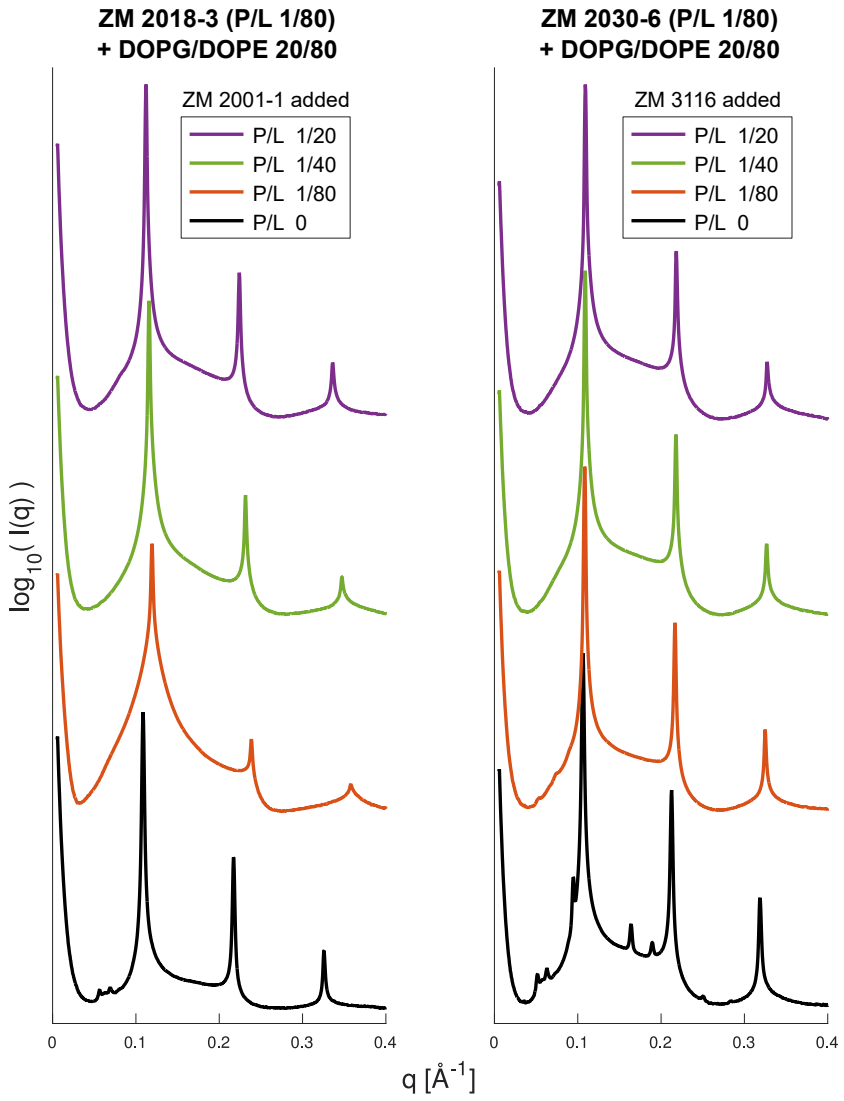

Figure 1.4: **NGC Abrogation by Gram Negative Selective Polymers**
SAXS data for mixtures of Gr+ selective polymer, Gr− selective polymer, and lipid vesicles of composition DOPG/DOPE 20/80. Gr+ selective polymer (as listed above each plot) is present at a constant protein to lipid (P/L) molar ratio of 1/80 for all plots. Gr− selective polymer (as specified in the legend) is added at the P/L ratio indicated.

1.3 Conclusion

In summary, this system of polyoxazoline-based random copolymers mimics the action of natural antimicrobial peptides and yields insight into mechanisms for targeting Gram-positive and Gram-negative bacteria. Bacterial killing assays reveal that a complete reversal in bacterial selectivity can be induced by tuning the ratio of hydrophilic and hydrophobic residues in the polymer. SAXS results suggest that polymer variants operate through two mechanisms: hydrophilic variants through a NGC-generating mechanism and hydrophobic variants through a NGC-independent mechanism. Additionally, the affinity between polymers and bacterial membranes can be more finely tuned by adjusting the volume occupied by the particular hydrophobic residue. The relationship between hydrophobicity and bacterial selectivity found in this study need not be universal for antimicrobial peptides or synthetic antimicrobials. Rather, this set of synthetic polymers provides a platform in which the effects of hydrophobicity and charge are isolated from potential interference by other physiochemical parameters. Their effects can then be investigated independently in order to elucidate the interactions between tunable polymer properties and the fundamental components of Gram positive and Gram negative bacteria.

1.4 Methods

1.4.1 Polyoxazoline Synthesis and MIC Assay

Polyoxazoline synthesis and MIC assays are performed as described in [32]. Briefly, monomers of each type (3-aminopropyl, *n*-butyl, *i*-butyl, *c*-butyl) are synthesized as derivatives of 2-oxazoline. Hydrophilic and hydrophobic monomers are mixed at the desired ratio and undergo a ring-opening polymerization to form the full poly(2-oxazoline) polymer. Bacteria are cultured for 9 hr in Luria-Bertani (LB) medium prior to resuspension in Mueller-Hinton (MH) broth at 2×10^5 CFU/mL in a 96-well plate. Poly(2-oxazoline) is then added to each

sample well at concentrations from 3.13 μg/mL to 400 μg/mL and the plate is incubated for a further 9 hr. Dose-dependent response curves are plotted based on the percentage of surviving bacterial cells in order to determine the MIC.

1.4.2 SAXS Lipid Sample Preparation

Small unilamellar vesicles (SUVs) were prepared by the following method. Lyophilized DOPS, DOPG, and DOPE (Avanti Polar Lipids) were dissolved in chloroform in 20 mg/mL stock solutions. Lipid compositions were formed by mixing stock solutions at the following molar ratios: DOPG/DOPE 20/80, DOPG/DOPE/DOPC 20/60/20, DOPS/DOPE 20/80. Chloroform was evaporated via N_2 gas followed by overnight desiccation under vacuum. Dried lipids were resuspended in physiological buffer (aqueous solution with 140 mM NaCl, 10 mM HEPES at pH 7.4) at a concentration of 20 mg/mL. Following overnight incubation at 37°C, lipid solutions were sonicated for 20 min (or until the solution became clear) to generate SUVs. Solutions were extruded through a 0.2 μm filter (Anotop) to ensure monodispersity in size. Solutions were stored at 4°C until use.

Synthetic polymers were dissolved in physiological buffer, then mixed with SUVs at the appropriate peptide/lipid molar ratios. Mixtures were shaken at low speed for 1 hr and allowed to equilibrate overnight. Precipitates from polymer-lipid mixtures were transferred to 1.5 mm quartz capillaries (Hilgenberg GmbH) and hermetically sealed with an oxygen torch.

1.4.3 SAXS Data Collection and Analysis

Prior to measurement, samples were centrifuged at 6000 rpm for 30 minutes. Samples were then measured at the Stanford Synchrotron Radiation Lightsource (SSRL) Beamline, 4–2. X-rays with energy 9 keV were fired at the sample, and scattered radiation was measured by a Pilatus 3X1M detector (pixel size 172 μm). The sample-to-detector distance was set

to 1.7 m. 2D Powder diffraction images were azimuthally integrated using the Nika package (version 1.82) for Igor Pro (version 7.04) and FIT2D [33, 34]. MATLAB (Mathworks) was used to plot scattering intensity $I(q)$ versus the momentum transfer q.

Structures of polymer/lipid complexes were solved by comparing measured q-positions of all peaks with permitted reflections for various phases. For lamellar phases, q-positions occur in a ratio $1:2:3:4:5:...$ and the lamellar spacing d is specified by the relation $q = dh$. For cubic phases, q-positions occur in the ratio $\sqrt{2}:\sqrt{3}:\sqrt{4}:\sqrt{6}:\sqrt{8}:...$ for Pn3m phases and $\sqrt{2}:\sqrt{4}:\sqrt{6}:\sqrt{8}:\sqrt{10}:...$ for Im3m phases. The lattice parameter a for both cubic phases is specified by $q = (2\pi/a)\sqrt{h^2+k^2}$. Both lattice parameters are extracted by assigning each observed peak a set of Miller indices (h, k) and performing a linear regression of momentum transfer q versus a function of Miller indices.

Section 2

Smoking and Immunomodulatory Complex Formation

2.1 Introduction

2.1.1 Autoimmune Diseases and TLR9 Hyperactivation

Autoimmune diseases are a class of disorders that involve the hyperactivation of the adaptive immune system in the absence of a detectable underlying pathology [35]. Despite the diversity of autoimmune disease etiologies, many arise from the disregulation of one or more soluble factors that typically facilitate the immune response. These include vasculitis, which results from the overexpression of tumor necrosis factor α (TNF–α), and systemic wasting syndrome, which results from the underexpression of transforming growth factor β (TGF–β) [35]. Treating autoimmune diseases often proves to be a complex affair. Cytokine-based treatments must be done with caution, as cytokines are often pleiotropic, having multiple or overlapping functions [36]. Additionally, a single cytokine can different effects depending on the stage of disease progression [35]. Immunosuppressants are also incorporated into autoimmune disease treatments, and have been effective in treating psoriasis and rheumatoid arthritis, among others [37]. Long term immunosuppresive treatment, however, can have adverse effects. For example, cyclosporin A (CsA), a widely used immunosuppresant, is associated with nephrotoxicity, renal vascular damage, and hypertension [38]. Thus investigation of the underlying physical phenomena behind autoimmune disease may be the key to developing more effective treatments.

Toll-like receptors (TLRs) are implicated in the pathogenesis of autoimmune diseases [39]. TLRs are a class of transmembrane proteins that recognize pathogen-associated molecular patterns (PAMPs), molecules or chemical motifs of foreign origin, as well as damage-associated molecular patterns (DAMPs), signals released from dead or dying cells [39, 40]. Each TLR recognizes a specific ligand (or set of ligands), and a successful ligand-receptor binding interaction initiates a signaling cascade that causes altered gene expression, ultimately resulting in the production of proinflammatory cytokines and interferons [39]. TLR9 is an endosomal TLR of particular interest in the context of autoimmune disease, as it is capable of recognizing double-stranded DNA (dsDNA) [40]. Under normal circumstances, TLR9 recognizes only bacterial dsDNA, which is distinguished from self-dsDNA by its abundance of cytosine-guanine repeats [41]. A chronic disease state, however, can produce conditions in which self-dsDNA associates with proteins or anti-DNA antibodies [42], forming a complex that is recognizable by TLR9. For example, in Systemic Lupus Erythematosus patients, neutrophils more frequently undergo a form of apoptosis in which the cell releases a neutrophil extracellular trap (NET): a network of antimicrobial peptides (AMPs) and extruded dsDNA [43].

Polycationic molecules and dsDNA can form complexes [44] that can participate in multivalent binding. The stability conferred by a multivalent binding interaction is orders of magnitude greater than that of an equivalent number of monovalent binding interactions [45]. Thus a single complex containing multiple dsDNA strands is able to recruit and form stable connections with several TLR9 molecules. However, the number of connections with TLR9 receptors (and thus the level of TLR9 activation), is strongly dependent on the organization of DNA within the complex. Small angle X-ray scattering (SAXS) reveals that certain polycations are able to organize DNA into structures with liquid-crystalline order, particularly those in which dsDNA strands are arranged in parallel columns [46]. If this arrangement is highly symmetric (e.g. forming a square or hexagonal lattice), each strand of dsDNA is located a distance d_{DNA} from adjacent strands, where d_{DNA} is known as the inter-DNA

spacing [46, 47]. Ostensibly, the maximal number of TLR9 molecules can be recruited when d_{DNA} matches the steric size of TLR9 ($\approx$ 3.5 nm). A d_{DNA} below 3.5 nm would make TLR9 clustering unfavorable due to steric repulsion, while a d_{DNA} above 3.5 nm would result in less efficient TLR9 clustering, as there would be "empty" space between receptors. In fact, this is confirmed by measuring type-I interferon production of murine macrophages exposed to DNA-AMP complexes of varying inter-DNA spacings: interferon production is maximal when d_{DNA} is approximately equal to the steric size of TLR9, and is lower otherwise [47]. Through various animal studies and cell stimulation assays, the link between liquid-crystalline ordering of DNA by the chemokine CXCL4 and TLR9 hyperactivation has been confirmed for systemic sclerosis [48]. Additional studies report analogous phenomena for the bacterial amyloid Curli [49] and Histone H4 in atherosclerosis [50].

2.1.2 Immunological Effects of Cigarette Smoke

Cigarette smoke has been linked to a number of health problems, including chronic obstructive pulmonary disease (COPD), atheroscleroris, and cancers of the lung, mouth, and larynx [51]. Surprisingly, a link also exists between smoking and autoimmune disease. Smoking has been shown to play a role in the pathogenesis of a number of autoimmune diseases, including systemic lupus erythematosus (SLE), rheumatoid arthritis (RA), and multiple sclerosis (MS) [52]. Additionally, the effects of autoimmune disease are sometimes exacerbated in smokers relative to nonsmokers [53]. Many proposed explanations for this have been offered. For example, smoking upregulates the expression of peptidylarginine deiminase (PAD) enzymes, which are responsible for protein citrillination [54]. Citrullinated proteins, in turn, serve as a marker for inflammation and are more abundant in patients with RA [55]. Additionally, due to the diversity of compounds released into the body during smoking, compounds can have competing effects. In MS patients, nicotine may reduce the severity of the disease, while other compounds increase promote demyelinisation, which is characteristic of the disorder [56].

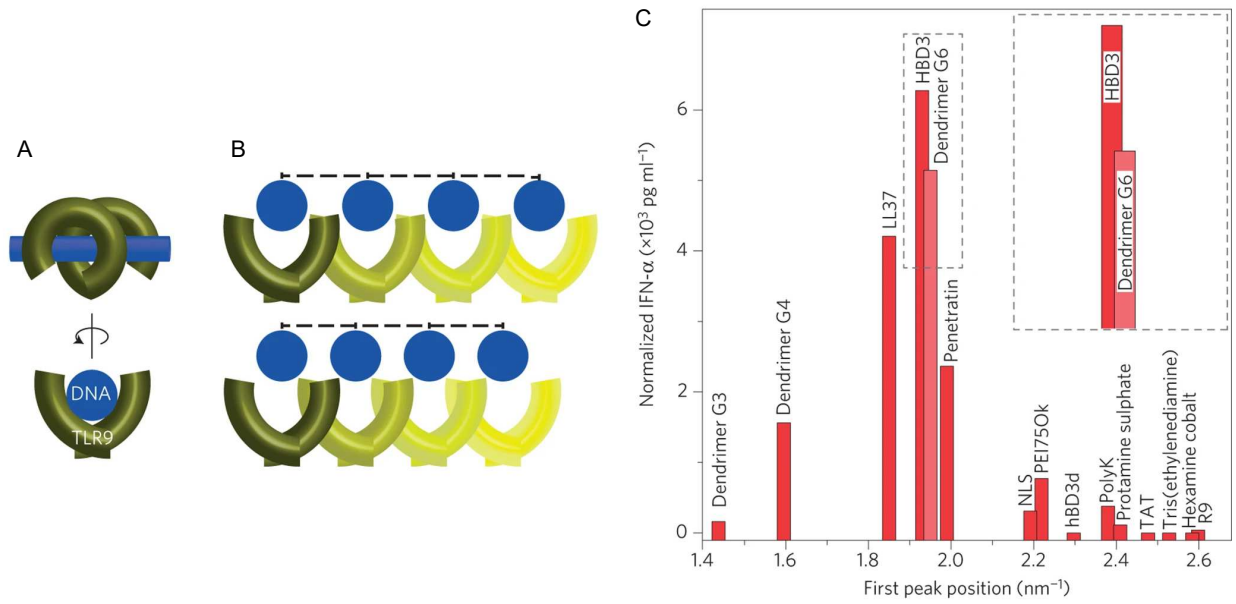

Figure 2.1: **Inter-DNA Spacing and TLR9 Hyperactivation**
(A) An illustration of the dsDNA-TLR9 complex from two perspectives. (B) Inter-DNA (d_{DNA}) spacing affects TLR9 clustering. When d_{DNA} is close to the steric size of TLR9 (≈3.5 nm), receptor clustering is optimal. Otherwise, the clustering is less efficient, either due to steric repulsion between receptors for relatively low d_{DNA} (bottom) or extra space between receptors for relatively high d_{DNA} (not shown). (C) Various compounds and antimicrobial peptides organize DNA into nanocrystalline structures with different d_{DNA}. Inter-DNA spacing affects production of the pro-inflammatory cytokine IFN-α. Cytokine production is maximal when the d_{DNA} is close to the steric size of TLR9, corresponding to a first peak position between 1.8 and 2.0 nm^{-1} (inset).

Is it possible that cigarette smoke contains compounds that promote DNA organization and subsequent TLR9 hyperactivation, culminating in the pathogenesis or exacerbation of autoimmune disease? Tobacco smoke contains over 1200 compounds, which include hydrocarbons, sterols, terpenes, carbohydrates, and alkaloids [57]. Out of these, cationic compounds (preferably polycationic) have the highest probability of organizing dsDNA. One such class of compounds found in tobacco smoke is alkaloids, nitrogen-containing organic compounds that constitute between 1.8-2.0% of cigarette filler component dry weight [58]. Nicotine is

the most common alkaloid found in tobacco, but other nicotine-derivatives are also present (Figure 2.2). At physiological pH (7.4), tobacco alkaloids present a combination of protonated (e.g. aliphatic, pyrrolidinyl, piperidinyl amines) and unprotonated (e.g. pyridinyl amines) functional groups. Additional compounds in cigarette smoke include butadiene, acrylamide, acrylonitrile, acrolein and acetaldehyde [57]. These compounds have the potential to polymerize upon burning or once in the body, incorporating or trapping alkaloids in the process. Taken altogether, this suggests the possibility of polycationic molecules or aggregates that, upon complexing with DNA, are capable of inducing inflammation via TLR9 hyperactivation.

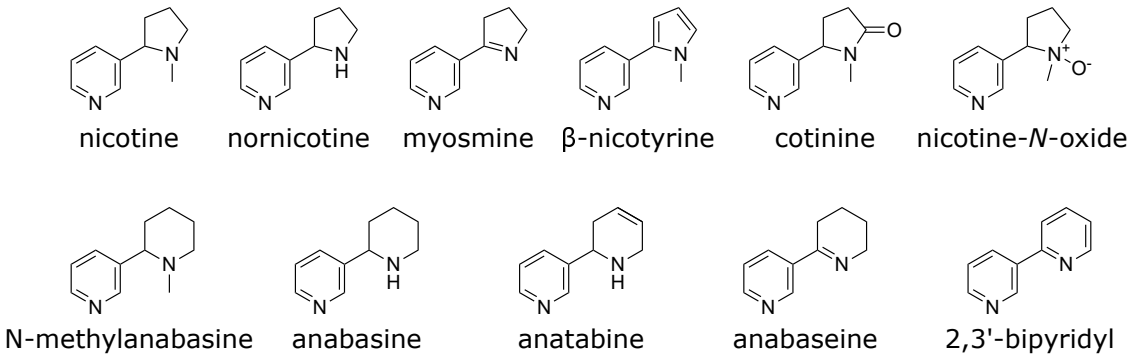

Figure 2.2: **Structures of Tobacco Alkaloids**
Nicotine is the dominant alkaloid in tobacco. Chemical structures of nicotine and nicotine-derived alkaloids found in tobacco are shown.

2.1.3 Synthetic Polymers for Investigating Inflammation

The potential for polycationic cigarette smoke compounds to organize DNA into immunomodulatory complexes makes synthetic tobacco mimics an excellent system for investigating the mechanism behind smoking-induced hyperinflammation. Monomers that mimic tobacco alkaloids (Figure 2.3) can be polymerized to form polycationic compounds. These include pyrrolidinyl propylmethacrylate (PyrMA), piperidinyl propylmethacrylate (PipMA), 4-vinylpyridine (4VP), and 2-vinylpyridine (2VP). Through free-radical polymerization, these monomers can be linked to form a variety of homopolymers and copolymers. Physiochemical

characteristics of each polymer, such as charge and charge density, can be controlled by the combination of monomers used as well as their stoichiometry. Molecular weight and polydispersity can be controlled through the use of chain transfer agents (e.g. mercaptoethanol) in conjunction with fractionation. The diversity of compounds in cigarette smoke, as well as the heterogeneity within individual samples, makes the investigation of cigarette smoke difficult. In contrast, this synthetic polymer system allows for the investigation of inflammatory processes modulated by smoking in a controllable and well-characterized system.

The use of synthetic polymers for mimicking pro-inflammatory compounds suggests another potential application: the development of polymers that lessen inflammation. Ideally, these polymers would not induce an inflammatory response on their own and would outcompete tobacco compounds for binding with DNA. Furthermore, when complexed with DNA, the inter-DNA spacing should fall outside the inflammatory range, namely far from the steric size of TLR9. Glucosamine-based glycopolymers represent one class of molecules that may fulfill these requirements. Bacterial sugars, such as mannose, can be detected by the immune system via specialized receptors [59]. In contrast, glucosamine is not a foreign saccharide and has been shown not to induce any serious or fatal side effects [60]. Glucosamines and *N*-acetyl glucosamines also have the potential to be cationic, which increases the probability of binding DNA and forming ordered complexes. If SAXS reveals that a particular glycopolymer produces an undesirable inflammatory inter-DNA spacing, parameters such as molecular weight distribution, hydrophobicity, chain architecture, and charge density can be tuned as desired until a desirable spacing is achieved.

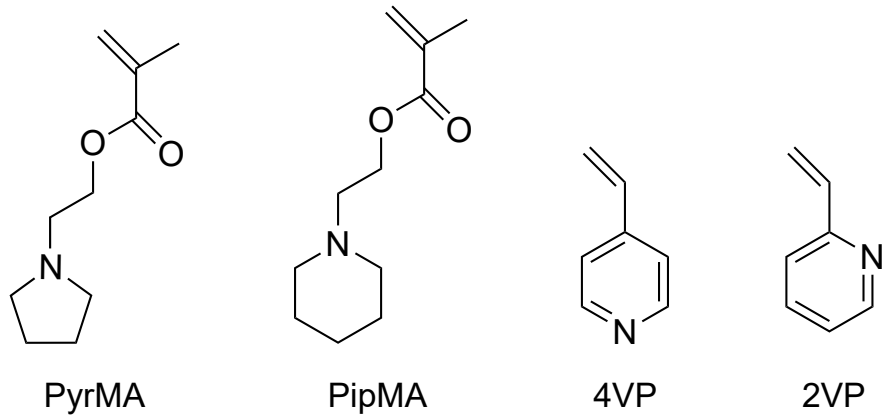

Figure 2.3: **Structures of Monomeric Tobacco Alkaloid Mimics**
Pyrrolidinyl propylmethacrylate (PyrMA), piperidinyl propylmethacrylate (PipMA), 4-vinylpyridine (4VP), and 2-vinylpyridine (2VP) are commercially available or synthesizable monomers and can be linked via free radical polymerization to form tobacco mimic polymers.

2.2 Results and Discussion

2.2.1 Heterogeneity of Tobacco Total Particulate Matter

One method of investigating the compounds introduced during smoking is by analyzing the composition of filter pads containing tobacco total particulate matter (TPM). These filter pads trap TPM during the process of machine smoking, as described by ISO standard 4387:2000. Prior to mixing with DNA, solid TPM must first be dissolved in an appropriate solvent. To investigate the possibility of possible TPM-induced DNA organization, TPM extracts in water, dimethyl sulfoxide (DMSO) and glacial acetic acid (AcOH) were combined with DNA at various TPM/DNA mass ratios. For the vast majority of TMP-DNA compositions, no visible precipitate was formed upon mixing (a common sign of macromolecular complex formation). Overall, it was found that TPM extracted from filter pads is unable to organize DNA to a significant degree: SAXS data reveals an absence of correlation peaks, indicators of periodicity within the sample.

This absence of detectable DNA organization may be attributed to the heterogeneity of

TPM, as TPM is comprised of a mixture of cationic, neutral, and anionic compounds. In order to accumulate sufficient cationic material, electrostatic complex formation would likely occur in compositions that contain excess TPM. However, DNA concentration in the sample decreases with increasing amounts of TPM, a condition that reduces the probability of complex formation. Diffraction features from DNA samples are typically weaker than their lipid counterparts (refer to Figure 1.4), thus any organization of DNA may be obfuscated by the heterogeneity of the TPM.

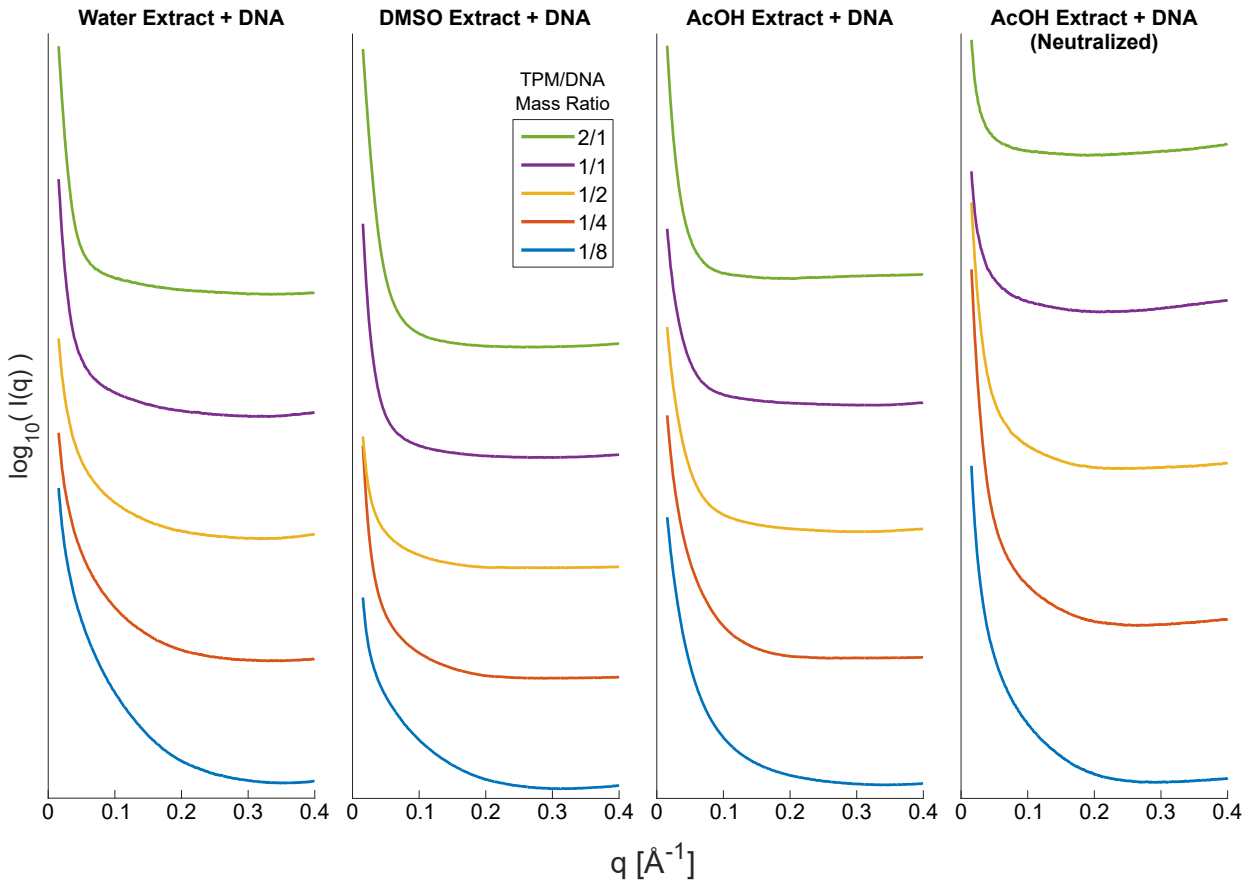

Figure 2.4: **SAXS of Tobacco TPM - DNA Complexes**
Tobacco total particulate matter (TPM) is extracted from a filter pad using various solvents: water, dimethyl sulfoxide (DMSO), and glacial acetic acid (AcOH). "Neutralized" indicates that the extract was neutralized to pH 7.0 prior to mixing with DNA. Plots show integrated intensity of SAXS data for mixtures of TPM extract and DNA at various TPM/DNA mass ratios. No correlation peaks were detected, despite the formation of condensates upon mixing TPM and DNA in some samples.

2.2.2 Complex Formation from Gas Washing

Gas washing represents another method of obtaining cigarette smoke compounds that more closely emulates the physiological process that occur during smoking. Ambient air is drawn through a cigarette and into a buffer solution to simulate inhalation and the deposition of cigarette smoke compounds within the body (refer to Section 2.4.1 and Figure 2.8A for details). Buffers at two different pH values were used: a pH 7.4 buffer (140 mM NaCl, 10 mM HEPES) to represent physiological conditions as well as a pH 5.0 buffer (140 mM NaCl, 10 mM Acetate) to represent the acidic conditions of the endosome, where TLR9 is found. At both pH levels, solutions with and without DNA were tested.

Cigarettes smoked into DNA-containing solutions yielded low-density precipitates. Precipitate formation was observed at both pH levels in DNA-containing solutions (see Figure 2.5C), but in neither of the buffer-only control solutions. SAXS was then used to investigate ordering within the precipitates. At pH 5.0, a DNA correlation peak was measured at $q_1 = 0.144\text{Å}^{-1}$ (Figure 2.5A,B). At pH 7.4, despite the presence of precipitates, no correlation peaks were observed in the SAXS results. Likewise, no correlation peaks were observed in samples without DNA.

It should be noted that a single correlation peak gives only an approximation of inter-DNA spacing, as a more accurate value would require additional peaks that specify the complete phase behavior. Without more correlation peaks, the geometry of the nanocrystalline structure cannot be fully specified. This is especially true of heterogeneous samples, such those produced through solvent extraction and gas washing, in which the precise mixture of compounds in the sample is unknown. For more well-characterized systems, such as the tobacco mimic polymer and glycopolymer complexes, the identities of compounds in the sample and their concentrations are known. The uncertainty due to the presence of a single peak, however, still remains. Ultimately, the notion inter-DNA spacing requires the presence of a symmetric columnar lattice of DNA. The singular peak does not provide evidence for the

existence of such a lattice, thus no inter-DNA spacing can be strictly defined for this system. The inter-DNA spacing, however, can still be estimated by assuming a lattice structure: the correlation peak at 0.144Å^{-1} suggests an inter-DNA spacing of 4.4 nm for a square columnar lattice and 5.0 nm for a hexagonal columnar lattice.

Overall, gas washing emulates the physiological process of smoking and suggests that organization of DNA by cigarette smoking compounds is feasible. The improved capability to generate liquid crystalline order at pH 5.0 is expected, as the higher concentration of protons would increase the polymer charge. Additionally, the higher linear charge density at pH 5.0 would better approximate the charge density of DNA, which in turn would make electrostatic complex formation more likely. Unorganized DNA complexes may be present in the extracellular space, and it may require endocytosis followed by the subsequent acidification of the endosome to produce order in the structure that would be necessary for TLR9 hyperactivation. As with TMP solvent extracts, samples produced through gas washing are quite heterogeneous. The observed correlation peak may be the result of multiple polycations assembling DNA. Alternatively, within this group of polycations, it is possible that a single species is primarily responsible for organizing DNA.

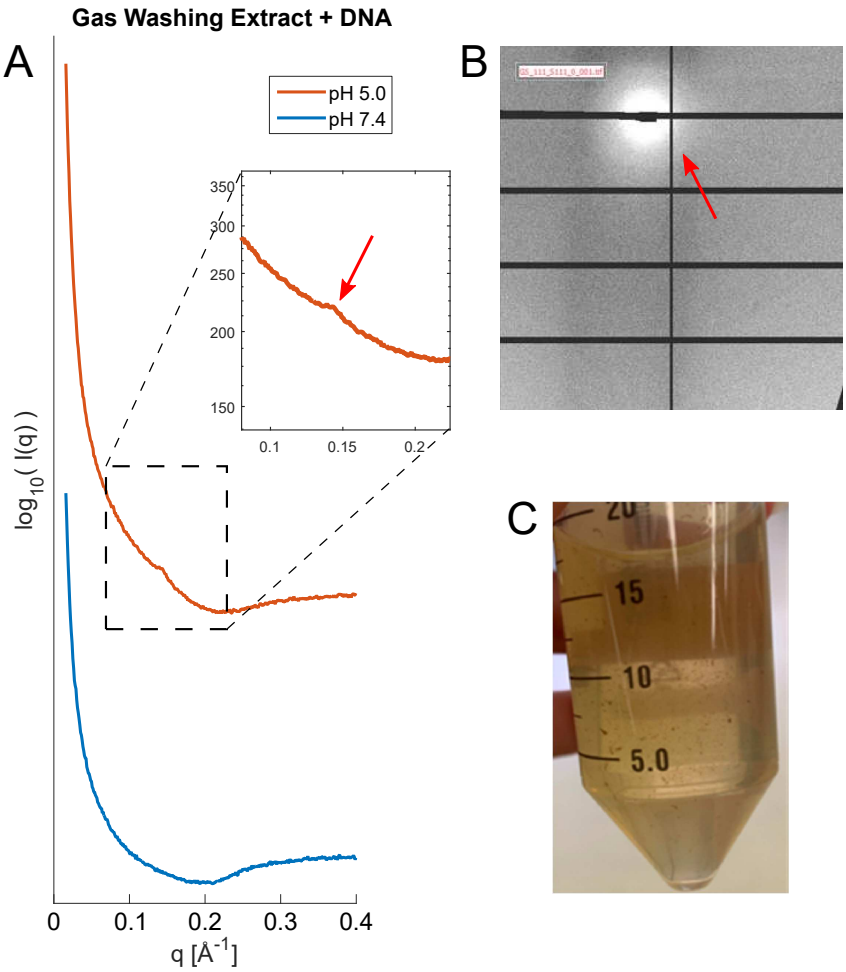

Figure 2.5: **SAXS of Gas Washing Extract - DNA Complexes**
Samples shown contain cigarette smoking compounds and DNA at a mass ratio of approximately 1/1. At pH 5.0, the correlation peak at $q_1 = 0.144 Å^{-1}$ demonstrates that the precipitates formed during gas washing have the ability to weakly organize DNA. Correlation peak (A, inset) and corresponding diffraction intensity maxima (B) are shown with red arrows. Diffraction image is contrast adjusted. No correlation peaks are observed at pH 7.4. Complexes appear as small, brown precipitates in solution (C).

2.2.3 Complex Formation from Tobacco Mimic Polymers

The synthesis of tobacco mimic polymers allows us to investigate the possibility of polycation-induced organization of DNA through the incorporation of chemical motifs similar to those found on tobacco alkaloids. Based on the starting monomers (Figure 2.3), the following tobacco mimics were synthesized and investigated: poly(4-vinylpyridine) (P4VP), Poly(2-vinylpyridine) (P2VP), poly(pyrrolidinyl propylmethacrylate) (Poly(PyrMA)), and poly(piperidinyl propylmethacrylate) (Poly(PipMA). Polymers were dissolved in DMSO and combined with DNA at various polymer/DNA (P/DNA) charge ratios for both pH 7.4 and pH 5.0. The implementation of charge ratios reflects the electrostatic interaction that drives DNA condensation; mass ratios are used when samples are heterogeneous, namely those in which the cationic charge density of the compound is unknown.

Precipitates were formed for the majority of polymer and DNA compositions. However, precipitates were also generated in samples without DNA, indicating that precipitate formation may be partly driven by the change in polymer solubility from pure DMSO to a DMSO/H_2O mixture. At pH 5.0, correlation peaks occurred for two compositions: P4VP + DNA at P/DNA = 1/2 and Poly(PipMA) + DNA at P/DNA = 2/1. Both correlation peaks were measured at $q_1 = 0.220\text{Å}^{-1}$. As with gas washing samples, the singular correlation peak does not provide sufficient structural information to deduce the inter-DNA spacing, but one can be estimated nonetheless. For instance, the correlation peak at 0.220Å^{-1} suggests an inter-DNA spacing of 2.9 nm for a square columnar lattice and 3.3 nm for a hexagonal columnar lattice. At pH 7.4, no correlation peaks were observed.

As with gas washing samples, tobacco mimic polymers demonstrate the ability to organize DNA. At pH 5.0, P4VP and P2VP contain more protonated amines relative to pH 7.4 (pyridinyl $pK_a \sim 5.2$). In contrast, Poly(PyrMA) and Poly(PipMA) contain similar amounts of protonated amines at both pH levels (pyrrolidinyl and piperidinyl $pK_a \sim 11$). Overall, the increased cationic charge of the polymers at pH 5.0 correlates with their ability to form or-

dered complexes with DNA. Since this is a shared feature of tobacco mimic and gas washing systems, the necessity of lower pH for DNA organization may potentially be applicable to cigarette smoke compounds in general. However, future experiments would be necessary to determine the nanocrystalline structure more precisely. If the resulting structure is a columnar hexagonal lattice, the inter-DNA spacing of 3.30 nm would represent an "inflammatory spacing", as it falls within the range of values known to hyperactivate TLR9, 3.0 – 4.0 nm. This would be consistent with the paradigm of smoking compounds exacerbating inflammation [47]. If, instead, the resulting structure is a columnar square lattice, the inter-DNA of spacing of 2.8 nm would imply an anti-inflammatory or non-inflammatory spacing. Since tobacco compounds can have competing effects [56], the tobacco mimic polymer may represent a subset of compounds or functional groups that prevent inflammation. The compound or chemical motif that is responsible for increased inflammation may be among those that have not been investigated through this system of synthetic tobacco alkaloid mimics.

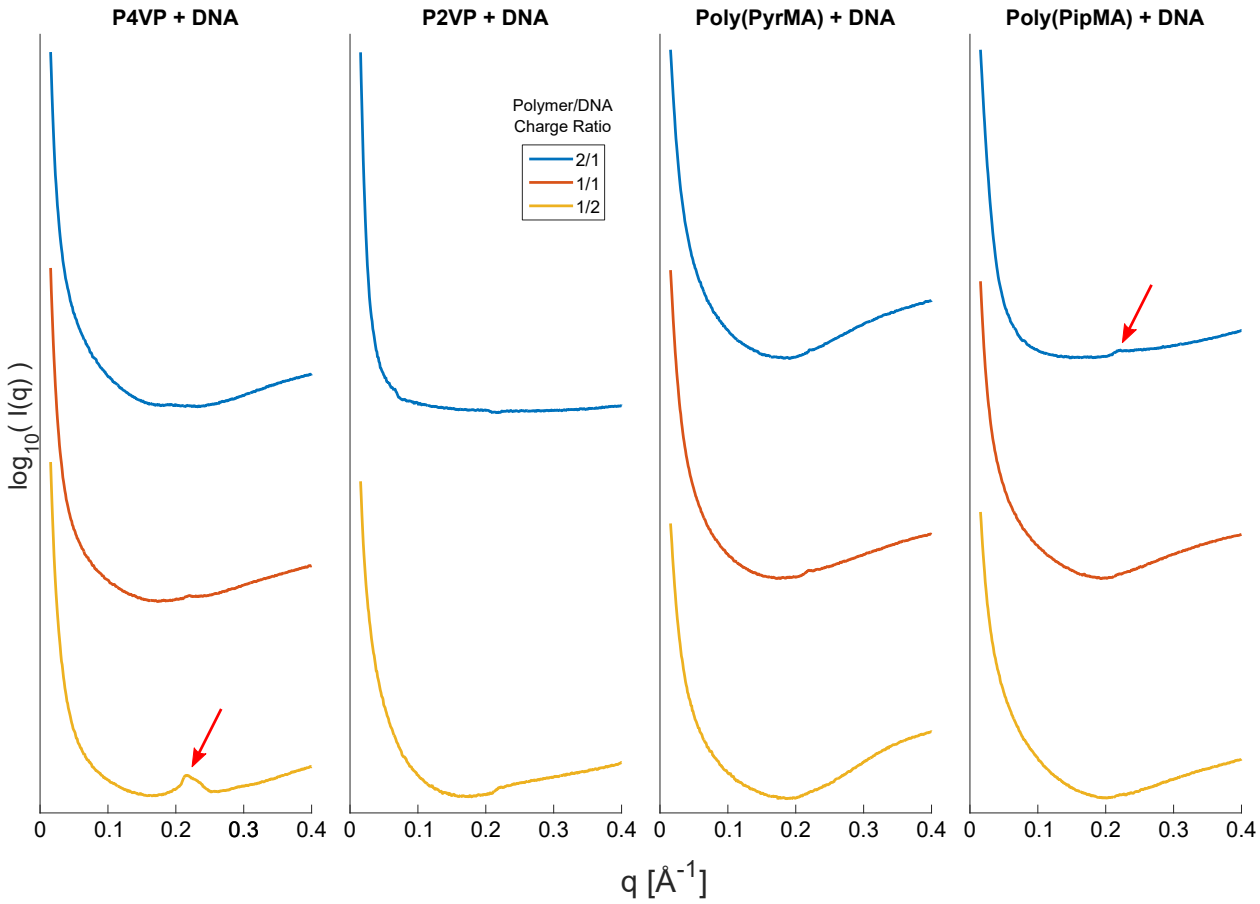

Figure 2.6: **SAXS of Tobacco Mimic Polymer - DNA Complexes**
DNA is mixed with various synthetic tobacco mimic polymers at the specified polymer to DNA charge ratios at pH 5.0. Plots are shown for mixtures of DNA with poly(4-vinylpyridine) (P4VP), Poly(2-vinylpyridine) (P2VP), poly(pyrrolidinyl propylmethacrylate) (Poly(PyrMA)), and poly(piperidinyl propylmethacrylate) (Poly(PipMA)). Red arrows indicate the location of correlation peaks (both at $q_1 = 0.220\text{Å}^{-1}$). No correlation peaks were observed for samples at pH 7.0 (not shown).

2.2.4 Glycopolymers Form Highly-Ordered Complexes with DNA

The primary glucosamine-based glycopolymer used in this study was poly(methyl 6-acryloyl-β-D-glucosaminoside) (poly(M6AG)). The structure is shown in Figure 2.7A. To investigate potential effects of molecular weight, various fractions are tested, namely those with number-average molecular weights (MW_n) of 44.2, 36.8, 20.0, 10.1, and 3.5 kDa. These represent number average degrees of polymerization of 179, 149, 81, 41, and 14, respectively. The 20.0 kDa fraction is of particular interest, as it is able to form a variety of structures with different lattice parameters.

Surprisingly, DNA organization was observed at both pH 7.4 and pH 5.0. At pH 7.4, broad peaks are present in only a subset of samples. For the 20.0 kDa fraction, correlation peaks were measured for polymer/DNA (P/DNA) charge ratios of 1/1 and 1/2, at $q_1 = 0.147 Å^{-1}$ and $q_1 = 0.158 Å^{-1}$, respectively (Figure 2.7B). As before, these single peaks cannot provide precise phase information. An inter-DNA spacing of 4.0–5.0 nm can be estimated, though the presence of a columnar lattice is not guaranteed. At pH 5.0, the majority of samples exhibit multiple sharp correlation peaks, indicative of a crystal domain size larger than that present at pH 7.4. The most prominent peaks likely give information about 2 dimensional ordering. For the 20.0 kDa fraction, the most prominent peaks suggest the presence of a hexagonal lattice with a=4.0 nm at P/DNA = 2/1, a hexagonal lattice with a= 3.5 nm at P/DNA = 1/1, and a tetragonal lattice with a=2.9 nm at P/DNA = 1/2 (Figure 2.7B–D). The lattice parameter a specifies the in-plane ordering of DNA columns (i.e. the inter-DNA spacing), while the lattice parameter c describes the periodicity of the lattice out of the plane (along a DNA column). Ordinarily, it can be assumed that $c \to \infty$, as the length of a DNA strand (c) is much larger than the spacing between DNA strands (a). However, the presence of smaller peaks together with the prominent peaks suggests that c is on the order of a, and thus cannot be neglected. Unfortunately, there is an insufficient amount of small peaks to adequately deduce the out-of-plane ordering.

Overall, this glycopolymer system demonstrates the ability to organize DNA effectively. Relative to the tobacco mimic polymers and gas washing extracts, poly(M6AG) can form organized complexes with DNA at both pH 7.4 and pH 5.0. This is consistent with the expected presence of protonated amines at both pH levels (poly(M6AG) $pK_a \sim 6.6$). Additionally, the more prominent and narrow peaks formed by poly(M6AG) suggest the presence of more crystals containing a larger number of repeat units. Together, these suggest that poly(M6AG) may be able to outcompete tobacco compounds for binding to DNA. For samples at lower pH, the presence of multiple correlation peaks is indicative of more highly-symmetric structures, increasing the probability that the assumed lattice parameters correspond to actual inter-DNA spacings. This, in turn, allows us to predict the level of inflammation that will result from glycopolymer-DNA induced TLR9 hyperactivation. Since the inter-DNA spacings fall within the inflammatory range of 3.0–4.0 nm, further tuning of glycopolymer parameters is required. Alternatively, since stoichiometry has been shown to affect both the crystal structure and lattice parameters, it must be a primary consideration. In practice, the combination of glycopolymer with DNA may need to be performed prior to administration in order to ensure that the desired stoichiometries are achieved without interference from other compounds that may be present in a heterogeneous environment. Overall, the use of glycopolymers serves as a promising method of reducing inflammation.

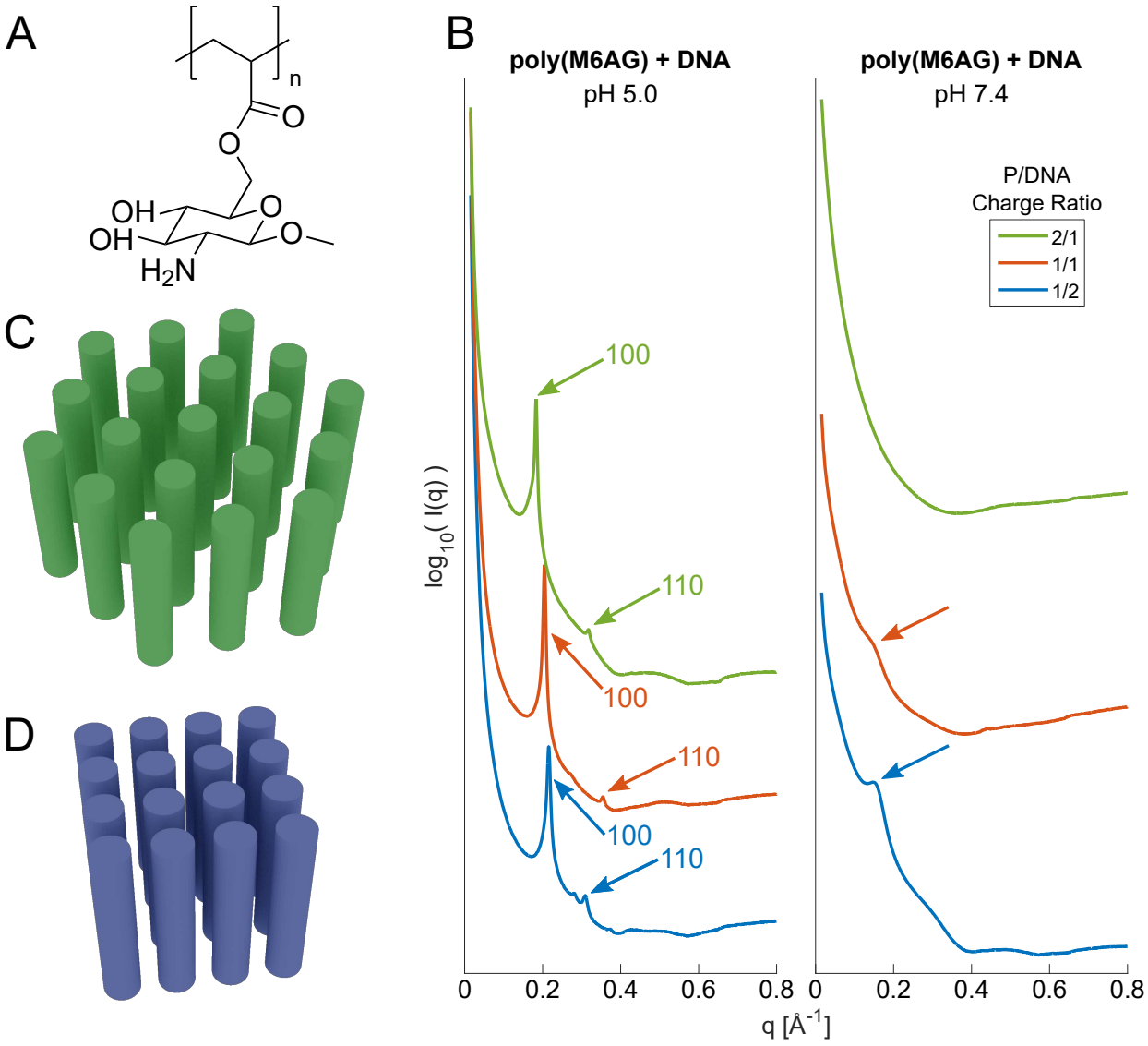

Figure 2.7: **SAXS of Glycopolymer - DNA Complexes**
(A) Chemical structure of poly(methyl 6-acryloyl-β-D-glucosaminoside) (poly(M6AG)). (B) SAXS of poly(M6AG) combined with DNA at the specified P/DNA charge ratios. For pH 5.0, arrows indicate the positions of correlation peaks that provide information about in-plane ordering of DNA. Miller indices (hk) are also indicated. For pH 7.4, arrows indicate the position of single correlation peaks. (C) Illustration of a columnar hexagonal phase with a = 4.0 nm, as in poly(M6AG) + DNA, pH 5.0, P/DNA = 2/1. (D) Illustration of a columnar tetragonal lattice with a = 2.9 nm, as in poly(M6AG) + DNA, pH 5.0, P/DNA = 1/2. For (C) and (D), columns represent strands of dsDNA with a diameter of 2.0 nm.

2.3 Conclusion

To summarize, a number of cognate systems can be used to investigate smoking-induced inflammation: solvent extraction of tobacco TPM, collection of smoke compounds by gas washing, and the synthesis of tobacco mimic polymers. Each approach illustrates the compromise between accurately simulating the biological and chemical aspects of smoking and developing a system that is controllable and well-characterized. For the gas washing and tobacco mimic polymer systems, SAXS reveals the formation of partially ordered complexes upon mixing with DNA. For samples obtained through solvent extractions, the heterogeneity of the tobacco TPM dominates, preventing the formation and/or detection of ordered macromolecular complexes. The ability of tobacco compounds to organize DNA also appears to be pH-dependent: organization of DNA at pH 7.4 was not observed, but such organization occurred for certain compositions at pH 5.0, simulating the acidified environment in the endosome where TLR9 is located. The data suggest that TLR9 clustering and hyperactivation, facilitated by the formation of properly-spaced molecules of DNA within a complex, may contribute to the overall mechanism by which smoking exacerbates or causes autoimmune disease. Furthermore, glycopolymers present a promising solution to reducing inflammation brought about by this TLR9 hyperactivation mechanism. Their mimicry of host saccharides and strong DNA binding and organization abilities highlight their potential utility in this system. For both tobacco mimic polymers and glycopolymers, additional refinements to the polymer synthesis methods will grant more control over relevant characteristics such as molecular weight and charge, allowing for the simulation of a wider range of polymer-DNA interactions.

2.4 Methods

2.4.1 Polymer Synthesis and Tobacco Extraction Methods

Briefly, the monomeric starting materials pyrrolidinyl propylmethacrylate (PyrMA), piperidinyl propylmethacrylate (PipMA), 4-vinylpyridine (4VP), and 2-vinylpyridine (2VP) undergo a free radical polymerization in toluene with 0.01 equivalents of radical initiator Azobisisobutyronitrile (AIBN). Two main methods are used to extract cigarette smoking compounds: gas washing and solvent extraction. In gas washing, a Dreschel bottle filled with 10 mL buffer (either 140 mM NaCl, 10 mM HEPES, pH 7.4 or 140 mM NaCl, 10 mM Acetate, pH 5.0). A reference cigarette (University of Kentucky) is lit and placed at the inlet, while a 60 mL plastic syringe (BD) is placed at the outlet. The syringe plunger is extended, drawing outside air through the cigarette, then into the buffer inside the Dreschel bottle, and finally into the syringe. Once the syringe is full, the syringe is detached from the apparatus, its contents are released, and the empty syringe is reinserted. This process is repeated until the cigarette is depleted, and additional cigarettes are smoked through the system until the desired mass of smoking compounds is deposited into the buffer ($\approx$ 1 mg per cigarette). Gas washing is illustrated in Figure 2.8A. In solvent extraction, Cambridge filter pads containing tobacco total particulate matter (University of Kentucky) are placed in 2 mL of solvent, either aqueous or organic. After 48-72 hr, the filter pad is removed from solution. The mass of smoking compounds transferred to the solvent is determined by the change in filter pad mass. For glacial acetic acid extractions, the solution is neutralized to pH 7.0 before being combined with DNA. Solvent extraction is illustrated in Figure 2.8B–C. Glycopolymer pK_a was estimated from the pK_a of the monomer using MarvinSketch (ChemAxon).

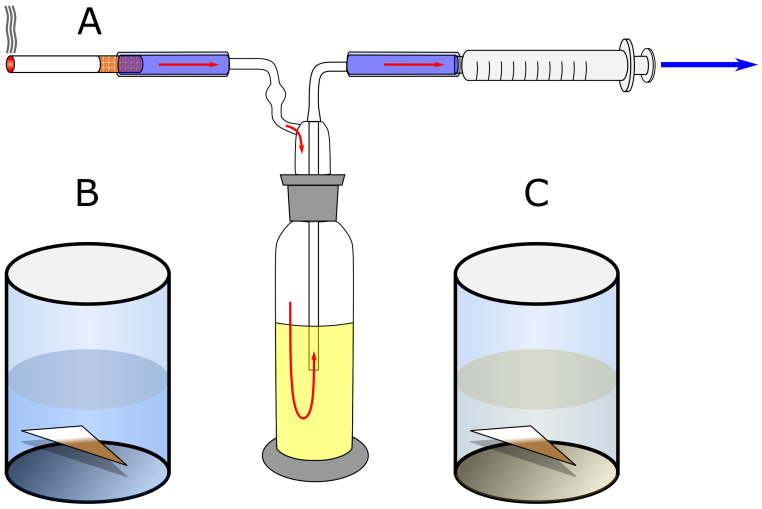

Figure 2.8: **Tobacco Extraction Methods**
Depictions of various methods used to extract tobacco smoke. (A) During gas washing, a lit cigarette and plastic syringe are arranged as shown, on either side of a Dreschel bottle filled with physiological buffer. Red arrows indicate the path of air flow when the syringe plunger is extended. Upon becoming filled, the syringe is detached and its contents are expelled, after which it is reattached. This process is repeated until the cigarette has been depleted. Alternatively, a tobacco filter pad can be placed inside a solution of water (B) or organic solvent (C).

Figure design by Brooke Jackson, University of California, Los Angeles.

2.4.2 SAXS DNA Sample Preparation

Calf thymus DNA is ethanol-precipitated and resuspended in aqueous buffer at either pH 7.4 (140 mM NaCl, 10 mM HEPES) or pH 5.0 (140 mM NaCl, 10 mM Acetate). Tobacco mimic polymers were dissolved in pH 7.4 or pH 5.0 buffer (or DMSO if insoluble in aqueous solution), then mixed with calf thymus DNA at the appropriate ratios. Charge ratios were used for sufficiently cationic polymers, otherwise molar ratios were used. For samples involving tobacco particulate matter, extracts were mixed with DNA at appropriate mass ratios.

Mixtures were shaken at low speed for 1 hr and allowed to equilibrate overnight. Precipitates from polymer-DNA mixtures were transferred to 1.5 mm quartz capillaries (Hilgenberg GmbH) and hermetically sealed with an oxygen torch.

2.4.3 SAXS Data Collection and Analysis

SAXS data collection, reduction, and analysis was performed as described in section 1.4.3, with the exception of the sample-to-detector distance being set to 1.7 m.

Inter-DNA spacing (equivalent to the lattice parameter a) can be deduced from the measured correlation peaks (q) and their corresponding miller indices: $q = \frac{2\pi}{a}\sqrt{h^2 + k^2}$ for a columnar square lattice and $q = \frac{4\pi}{\sqrt{3}a}\sqrt{h^2 + hk + k^2}$ for a columnar hexagonal lattice. When assuming a phase based on a single correlation peak at q_{10}, these simplify to $a = \frac{2\pi}{q_{10}}$ and $a = \frac{4\pi}{\sqrt{3}\cdot q_{10}}$, respectively.

References

[1] W. Kamysz, "Are antimicrobial peptides an alternative for conventional antibiotics?," *Nuclear medicine review. Central & Eastern Europe*, vol. 8, no. 1, pp. 78–86, 2005.

[2] C. Walsh, "Molecular mechanisms that confer antibacterial drug resistance," *Nature*, vol. 406, pp. 775–781, aug 2000.

[3] A. Giedraitiene, A. Vitkauskiene, R. Naginiene, and A. Pavilonis, "Antibiotic resistance mechanisms of clinically important bacteria," mar 2011.

[4] M. P. Jevons, "" Celbenin "-resistant Staphylococci," *British Medical Journal*, vol. 2, no. 5205, p. 1085, 1960.

[5] CDC, "Antibiotic resistance threats in the United States, 2019," tech. rep., National Center for Emerging Zoonotic and Infectious Diseases (U.S.), Atlanta, Georgia, nov 2019.

[6] M. Zasloff, "Antimicrobial peptides of multicellular organisms," *Nature*, vol. 415, no. 0028-0836 (Print), pp. 389–395, 2002.

[7] C. J. Jeffery, "Protein species and moonlighting proteins: Very small changes in a protein's covalent structure can change its biochemical function," *Journal of Proteomics*, vol. 134, pp. 19–24, feb 2016.

[8] W. L. Maloy and U. P. Kari, "Structure–activity studies on magainins and other host defense peptides," *Biopolymers*, vol. 37, no. 2, pp. 105–122, 1995.

[9] M. R. Yeaman and N. Y. Yount, "Mechanisms of Antimicrobial Peptide Action and Resistance," *Pharmacological Reviews*, vol. 55, no. 1, pp. 27–55, 2003.

[10] W. Vollmer, D. Blanot, and M. A. De Pedro, "Peptidoglycan structure and architecture," *FEMS Microbiology Reviews*, vol. 32, pp. 149–167, mar 2008.

[11] S. Brown, J. P. Santa Maria, and S. Walker, "Wall Teichoic Acids of Gram-Positive Bacteria," *Annual Review of Microbiology*, vol. 67, pp. 313–336, sep 2013.

[12] N. Malanovic and K. Lohner, "Antimicrobial peptides targeting Gram-positive bacteria," *Pharmaceuticals*, vol. 9, sep 2016.

[13] W. Vollmer and J. V. Höltje, "The architecture of the murein (peptidoglycan) in gram-negative bacteria: Vertical scaffold or horizontal layer(s)?," *Journal of Bacteriology*, vol. 186, pp. 5978–5987, sep 2004.

[14] M. Caroff and D. Karibian, "Structure of bacterial lipopolysaccharides," *Carbohydrate Research*, vol. 338, pp. 2431–2447, nov 2003.

[15] B. D. Needham and M. S. Trent, "Fortifying the barrier: The impact of lipid A remodelling on bacterial pathogenesis," *Nature Reviews Microbiology*, vol. 11, pp. 467–481, jul 2013.

[16] D. S. Snyder and T. J. McIntosh, "The lipopolysaccharide barrier: Correlation of antibiotic susceptibility with antibiotic permeability and fluorescent probe binding kinetics," *Biochemistry*, vol. 39, pp. 11777–11787, sep 2000.

[17] J. Li, J. J. Koh, S. Liu, R. Lakshminarayanan, C. S. Verma, and R. W. Beuerman, "Membrane active antimicrobial peptides: Translating mechanistic insights to design," *Frontiers in Neuroscience*, vol. 11, feb 2017.

[18] M. Spivak, *A Comprehensive Introduction to Differential Geometry (Volume 3)*. Publish or Perish, 3rd ed., 1999.

[19] N. W. Schmidt, A. Mishra, G. H. Lai, M. Davis, L. K. Sanders, D. Tran, A. Garcia, K. P. Tai, P. B. McCray, A. J. Ouellette, M. E. Selsted, and G. C. Wong, "Criterion for amino acid composition of defensins and antimicrobial peptides based on geometry of membrane destabilization," *Journal of the American Chemical Society*, vol. 133, pp. 6720–6727, may 2011.

[20] S. Dickson, "Minimal Surfaces," *Mathematica Journal*, vol. 1, pp. 38–40, 1990.

[21] E. A. Porter, B. Weisblum, and S. H. Gellman, "Mimicry of host-defense peptides by unnatural oligomers: Antimicrobial β-peptides," *Journal of the American Chemical Society*, vol. 124, pp. 7324–7330, jun 2002.

[22] N. P. Chongsiriwatana, J. A. Patch, A. M. Czyzewski, M. T. Dohm, A. Ivankin, D. Gidalevitz, R. N. Zuckermann, and A. E. Barron, "Peptoids that mimic the structure, function, and mechanism of helical antimicrobial peptides," *Proceedings of the National Academy of Sciences of the United States of America*, vol. 105, pp. 2794–2799, feb 2008.

[23] K. Kuroda, G. A. Caputo, and W. F. DeGrado, "The role of hydrophobicity in the antimicrobial and hemolytic activities of polymethacrylate derivatives," *Chemistry - A European Journal*, vol. 15, pp. 1123–1133, jan 2009.

[24] B. P. Mowery, S. E. Lee, D. A. Kissounko, R. F. Epand, R. M. Epand, B. Weisblum, S. S. Stahl, and S. H. Gellman, "Mimicry of antimicrobial host-defense peptides by random copolymers," *Journal of the American Chemical Society*, vol. 129, no. 50, pp. 15474–15476, 2007.

[25] G. S. Girolami, "A simple "back of the envelope" method for estimating the densities and molecular volumes of liquids and solids," *Journal of Chemical Education*, vol. 71, no. 11, pp. 962–964, 1994.

[26] S. J. Lam, N. M. O'Brien-Simpson, N. Pantarat, A. Sulistio, E. H. Wong, Y. Y. Chen, J. C. Lenzo, J. A. Holden, A. Blencowe, E. C. Reynolds, and G. G. Qiao, "Combating multidrug-resistant Gram-negative bacteria with structurally nanoengineered antimicrobial peptide polymers," *Nature Microbiology*, vol. 1, sep 2016.

[27] E. Jawetz, J. B. Gunnison, R. S. Speck, and V. R. Coleman, "Studies on antibiotic synergism and antagonism: The interference of chloramphenicol with the action of penicillin," *A.M.A Archives of Internal Medicine*, vol. 87, pp. 349–359, mar 1951.

[28] P. S. Ocampo, V. Lázár, B. Papp, M. Arnoldini, P. A. Zur Wiesch, R. Busa-Fekete, G. Fekete, C. Pál, M. Ackermann, and S. Bonhoeffer, "Antagonism between bacteriostatic and bactericidal antibiotics is prevalent," *Antimicrobial Agents and Chemotherapy*, vol. 58, pp. 4573–4582, aug 2014.

[29] P. Gionchetti, F. Rizzello, K. M. Lammers, C. Morselli, L. Sollazi, S. Davies, R. Tambasco, C. Calabrese, and M. Campieri, "Antibiotics and probiotics in treatment of inflammatory bowel disease," *World Journal of Gastroenterology*, vol. 12, pp. 3306–3313, jun 2006.

[30] W. Li, Z. Yao, L. Sun, W. Hu, J. Cao, W. Lin, and X. Lin, "Proteomics analysis reveals a potential antibiotic cocktail therapy strategy for aeromonas hydrophila infection in biofilm," *Journal of Proteome Research*, vol. 15, pp. 1810–1820, jun 2016.

[31] S. Fischer, S. Kittler, G. Klein, and G. Glünder, "Impact of a Single Phage and a Phage Cocktail Application in Broilers on Reduction of Campylobacter jejuni and Development of Resistance," *PLoS ONE*, vol. 8, oct 2013.

[32] M. Zhou, Y. Qian, J. Xie, W. Zhang, W. Jiang, X. Xiao, S. Chen, C. Dai, Z. Cong, Z. Ji, N. Shao, L. Liu, Y. Wu, and R. Liu, "Poly(2-Oxazoline)-Based Functional Peptide Mimics: Eradicating MRSA Infections and Persisters while Alleviating Antimicrobial Resistance," *Angewandte Chemie - International Edition*, vol. 59, pp. 6412–6419, apr 2020.

[33] J. Ilavsky, "Nika: Software for two-dimensional data reduction," *Journal of Applied Crystallography*, vol. 45, pp. 324–328, feb 2012.

[34] F. Zhang, J. Ilavsky, G. G. Long, J. P. Quintana, A. J. Allen, and P. R. Jemian, "Glassy carbon as an absolute intensity calibration standard for small-angle scattering," *Metallurgical and Materials Transactions A: Physical Metallurgy and Materials Science*, vol. 41, pp. 1151–1158, may 2010.

[35] A. Davidson and B. Diamond, "Autoimmune diseases," *New England Journal of Medicine*, vol. 345, pp. 340–350, aug 2001.

[36] K. Ozaki and W. J. Leonard, "Cytokine and cytokine receptor pleiotropy and redundancy," *Journal of Biological Chemistry*, vol. 277, pp. 29355–29358, aug 2002.

[37] V. F. Quesniaux, "Immunosuppressants: Tools to investigate the physiological role of cytokines," *BioEssays*, vol. 15, pp. 731–739, nov 1993.

[38] A. M. De Mattos, A. J. Olyaei, and W. M. Bennett, "Nephrotoxicity of immunosuppressive drugs: Long-term consequences and challenges for the future," *American Journal of Kidney Diseases*, vol. 35, pp. 333–346, feb 2000.

[39] A. M. Hosseini, J. Majidi, B. Baradaran, and M. Yousefi, "Toll-like receptors in the pathogenesis of autoimmune diseases," *Advanced Pharmaceutical Bulletin*, vol. 5, no. Suppl 1, pp. 605–614, 2015.

[40] K. Takeda, T. Kaisho, and S. Akira, "Toll-Like Receptors," *Annual Review of Immunology*, vol. 21, pp. 335–376, apr 2003.

[41] A. Dalpke, J. Frank, M. Peter, and K. Heeg, "Activation of toll-like receptor 9 by DNA from different bacterial species," *Infection and Immunity*, vol. 74, pp. 940–946, feb 2006.

[42] S. R. Christensen, M. Kashgarian, L. Alexopoulou, R. A. Flavell, S. Akira, and M. J. Shlomchik, "Toll-like receptor 9 controls anti-DNA autoantibody production in murine lupus," *Journal of Experimental Medicine*, vol. 202, pp. 321–331, jul 2005.

[43] R. Lande, D. Ganguly, V. Facchinetti, L. Frasca, C. Conrad, J. Gregorio, S. Meller, G. Chamilos, R. Sebasigari, V. Riccieri, R. Bassett, H. Amuro, S. Fukuhara, T. Ito, Y. J. Liu, and M. Gilliet, "Neutrophils activate plasmacytoid dendritic cells by releasing self-DNA-peptide complexes in systemic lupus erythematosus," *Science Translational Medicine*, vol. 3, pp. 1–11, mar 2011.

[44] V. A. Bloomfield, "DNA condensation by multivalent cations," *Biopolymers*, vol. 44, pp. 269–282, jan 1997.

[45] D. J. Diestler and E. W. Knapp, "Statistical mechanics of the stability of multivalent ligand-receptor complexes," *Journal of Physical Chemistry C*, vol. 114, pp. 5287–5304, apr 2010.

[46] E. Y. Lee, C. K. Lee, N. W. Schmidt, F. Jin, R. Lande, T. Curk, D. Frenkel, J. Dobnikar, M. Gilliet, and G. C. Wong, "A review of immune amplification via ligand clustering by self-assembled liquid–crystalline DNA complexes," *Advances in Colloid and Interface Science*, vol. 232, pp. 17–24, jun 2016.

[47] N. W. Schmidt, F. Jin, R. Lande, T. Curk, W. Xian, C. Lee, L. Frasca, D. Frenkel, J. Dobnikar, M. Gilliet, and G. C. Wong, "Liquid-crystalline ordering of antimicrobial peptide-DNA complexes controls TLR9 activation," *Nature Materials*, vol. 14, no. 7, pp. 696–701, 2015.

[48] R. Lande, E. Lee, R. Palazzo, B. Marinari, I. Pietraforte, G. Santos, Y. Mattenberger, F. Spadaro, K. Stefanantoni, N. Iannace, A. Dufour, M. Falchi, M. Bianco, E. Botti, L. Bianchi, M. Alvarez, V. Riccieri, M. Truchetet, G. Wong, and L. Frasca, "CXCL4 assembles DNA into liquid crystalline complexes to amplify TLR9-mediated interferon-α production in systemic sclerosis," *Provisionally Accepted Nature Communications*, 2019.

[49] S. A. Tursi, E. Y. Lee, N. J. Medeiros, M. H. Lee, L. K. Nicastro, B. Buttaro, S. Gallucci, R. P. Wilson, G. C. Wong, and Ç. Tükel, "Bacterial amyloid curli acts as a carrier for DNA to elicit an autoimmune response via TLR2 and TLR9," *PLoS Pathogens*, vol. 13, pp. 1–25, apr 2017.

[50] C. Silvestre-Roig, Q. Braster, K. Wichapong, E. Y. Lee, J. M. Teulon, N. Berrebeh, J. Winter, J. M. Adrover, G. S. Santos, A. Froese, P. Lemnitzer, A. Ortega-Gómez, R. Chevre, J. Marschner, A. Schumski, C. Winter, L. Perez-Olivares, C. Pan, N. Paulin, T. Schoufour, H. Hartwig, S. González-Ramos, F. Kamp, R. T. Megens, K. A. Mowen, M. Gunzer, L. Maegdefessel, T. Hackeng, E. Lutgens, M. Daemen, J. von Blume, H. J. Anders, V. O. Nikolaev, J. L. Pellequer, C. Weber, A. Hidalgo, G. A. Nicolaes, G. C. Wong, and O. Soehnlein, "Externalized histone H4 orchestrates chronic inflammation by inducing lytic cell death," *Nature*, vol. 569, pp. 236–240, may 2019.

[51] D. G. Yanbaeva, M. A. Dentener, E. C. Creutzberg, G. Wesseling, and E. F. Wouters, "Systemic effects of smoking," *Chest*, vol. 131, pp. 1557–1566, may 2007.

[52] K. H. Costenbader and E. W. Karlson, "Cigarette smoking and autoimmune disease: What can we learn from epidemiology?," nov 2006.

[53] C. Perricone, M. Versini, D. Ben-Ami, S. Gertel, A. Watad, M. J. Segel, F. Ceccarelli, F. Conti, L. Cantarini, D. P. Bogdanos, A. Antonelli, H. Amital, G. Valesini, and Y. Shoenfeld, "Smoke and autoimmunity: The fire behind the disease," *Autoimmunity Reviews*, vol. 15, pp. 354–374, apr 2016.

[54] D. Makrygiannakis, M. Hermansson, A. K. Ulfgren, A. P. Nicholas, A. J. Zendman, A. Eklund, J. Gmnewald, C. M. Skold, L. Klareskog, and A. I. Catrina, "Smoking increases peptidylarginine deiminase 2 enzyme expression in human lungs and increases citrullination in BAL cells," *Annals of the Rheumatic Diseases*, vol. 67, pp. 1488–1492, oct 2008.

[55] D. Makrygiannakis, E. Af Klint, I. E. Lundberg, R. Löfberg, A. K. Ulfgren, L. Klareskog, and A. I. Catrina, "Citrullination is an inflammation-dependent process," *Annals of the Rheumatic Diseases*, vol. 65, pp. 1219–1222, sep 2006.

[56] Z. Gao, J. C. Nissen, K. Ji, and S. E. Tsirka, "The experimental autoimmune encephalomyelitis disease course is modulated by nicotine and other cigarette smoke components," *PLoS ONE*, vol. 9, sep 2014.

[57] R. L. Stedman, "The chemical composition of tobacco and tobacco smoke," *Chemical Reviews*, vol. 68, pp. 153–207, apr 1968.

[58] A. Eldridge, T. R. Betson, M. V. Gama, and K. McAdam, "Variation in tobacco and mainstream smoke toxicant yields from selected commercial cigarette products," *Regulatory Toxicology and Pharmacology*, vol. 71, pp. 409–427, apr 2015.

[59] U. Gazi and L. Martinez-Pomares, "Influence of the mannose receptor in host immune responses," jul 2009.

[60] J. W. Anderson, R. J. Nicolosi, and J. F. Borzelleca, "Glucosamine effects in humans: A review of effects on glucose metabolism, side effects, safety considerations and efficacy," *Food and Chemical Toxicology*, vol. 43, pp. 187–201, feb 2005.